Classical-equations-of-motion calculations of high-energy heavy-ion collisions

A. R. Bodmer and C. N. Panos*
Argonne National Laboratory, Argonne, Illinois 60439 and University of Illinois at Chicago Circle, Chicago, Illinois 60680

A. D. MacKellar
University of Kentucky, Lexington, Kentucky 40506

(Received 5 October 1979)

Results are obtained with the classical-equations-of-motion approach which provides a complete microscopic, classical, description including finite-range interaction effects. Nonrelativistic classical-equations-of-motion calculations are made for equal mass projectile and target nuclei with $A_P = A_T = 20$ (Ne + Ne) at laboratory energies per projectile nucleon of $E_L = 117$, 400, and 800 MeV and at 400 MeV for $A_P = A_T = 40$ (Ca + Ca). A static two-body potential V_{st} is used which is fitted to $\sigma^{(2)}$, the $\sin^2\theta$ weighted differential cross section. For $A_P = A_T = 20$ we also use a scattering equivalent momentum dependent potential V_{tr}. V_{st} and V_{tr} give identical two-body scattering but are not equivalent for many-body scattering and are used to test for finite-range interaction effects in heavy-ion collisions. The evolution of central collisions is discussed. For these multiple scattering is large leading to high momentum components. Dissipation quite generally is larger at lower energies and is appreciable during the expansion phase of central collisions giving approximately thermalized distributions at the lower E_L. A peak at approximately the same momentum at all angles develops in the momentum distribution near the beginning of the expansion and changes roughly in step with the potential energy; for $A_P = A_T = 20$ at 800 MeV the peak persists to the final distributions. There are very appreciable differences in the densities, potential energies, and distributions between V_{st} and V_{tr} during the strong interaction stage. However, the final distributions are not significantly different even for $A_P = A_T = 20$ at 800 MeV. For $A_P = A_T = 40$ at 400 MeV a transverse peaking develops in the momentum distribution suggestive of collective effects. Noncentral collisions show typical nonequilibrium features and for larger impact parameters the final distributions show a strong single scattering component. This is true also of the impact parameter averaged distributions which are in fair agreement with experiment. A partial test of thermal models is made. Limitations and extensions of the classical-equations-of-motion approach are discussed. In particular we propose a new kinetic equation which includes finite-range interaction effects. Relativistic classical-equations-of-motion calculations to $O(v^2/c^2)$ are briefly discussed.

[NUCLEAR REACTIONS Heavy ion (Ne+ Ne, Ca+ Ca); laboratory energy/n = 117, 400, 800 MeV; classical microscopic many-body calculations.]

I. INTRODUCTION

We present and discuss results obtained for high-energy heavy-ion (HE-HI) collisions[1] with the classical-equations-of-motion (CEOM) approach. The essence of this microscopic approach is the classical calculation of all $A = A_P + A_T$ trajectories (A_P, A_T are the projectile and target mass numbers, respectively) using a two-body potential between all pairs of nucleons.[2-5] The results of the trajectory calculations are subsequently analyzed and averaged over an ensemble of initial configurations of positions and momenta representing the initial nuclei. The input is the free nucleon-nucleon cross section and also, in principle, the binding and saturation properties of nuclei.

For laboratory energies $E_L \lesssim 1$ GeV/A_P, i.e., for HE-HI collisions (as contrasted with relativistic heavy-ion collisions for $E \gtrsim 1$ GeV/nucleon), relativistic effects, apart from pion production, are only moderately important and it may be adequate to consider these to $O(v^2/c^2)$; furthermore, at the intermediate or lower energies in this range, pion production is not expected to be very important and relativistic corrections should be small. Even then, and without taking account of possible exotic states of nuclear matter,[6] the interpretation of HE-HI collisions poses formidable theoretical problems: The initial and final states for central collisions are very different; with a nucleon mean free path $\Lambda \approx 2$ fm one can expect large nonequilibrium, dissipative, and transparency effects; the densities may become quite large. A complete relativistic quantum mechanical approach is not possible and unfortunately there is no obviously justifiable simplification such as the time-dependent Hartree-Fock (TDHF) approach at lower energies (whose validity depends on a long mean-free path). This forces one to consider approaches which are classical, or, at best, semiclassical.

There are effectively three basic or *a priori* approaches, in distinction to a number of more phenomenological thermal models[7] which assume thermalization and also make geometrical assumptions. The three *a priori* approaches are each associated with certain approximations. They have been anal-

yzed and compared[8,9] and are summarized below in order of increasingly microscopic descriptions.

A. Hydrodynamics ("macroscopic" description)[10]

This requires $\Lambda/L \ll 1$ for its validity (Λ = mean free path, L = "macroscopic" length characteristic of a nucleus-nucleus collision). This condition implies local or approximately local thermal equilibrium, i.e., relaxation times ($\approx \Lambda/v$) sufficiently short compared to collision times ($\approx L/v$) so that approximate local equilibrium can be established. In fact, for HE-HI collisions one has $\Lambda/L \approx 0.2-0.5$ depending on the radii of the nuclei and whether the collisions are central or noncentral. This implies large dissipative and nonequilibrium effects and thus the probable need for a microscopic description, especially for lighter nuclei, and for noncentral collisions even for heavier nuclei. Λ/L not small compared to unity implies inherently large dissipation; thus if hydrodynamics is used one should use at least the Navier-Stokes equations since these include dissipation (viscosity and thermal conductivity).[8]

B. Intranuclear nuclear cascade calculations or equivalent Boltzmann-equation descriptions[11]

These are closely related to or, for Boltzmann-type equations, are microscopic kinetic-equation descriptions involving the one-particle distribution function $f(\vec{x}, \vec{p}, t)$. These approaches mostly require, in particular, that conditions be dilute, i.e., that $d/\Lambda \ll 1$ or equivalently $\rho d^3 \ll 1$ (ρ = particle number density, d = nucleon-nucleon force range).[12] Thus these descriptions imply the ideal-gas equation of state since all potential energy and finite range effects are neglected. However, no assumptions are made about equilibrium, and arbitrarily large nonequilibrium effects can be described through the full nonlinear collision term. These approaches effectively use the free NN cross section (this enters the collision term in the Boltzmann equation), and particle production and relativistic kinematics can readily be included. These approaches then provide an essentially unique microscopic description based on the free NN cross sections, but because of neglect of potential-energy effects they cannot include effects associated with a nontrivial (nonideal gas) equation of state. Also, they are inherently limited in the information they can give about correlations and composites.

At least for not too high energies ($\lesssim$1 GeV/nucleon), nuclear matter, especially for conditions near maximum overlap in central or near central collisions, is not dilute and $d/\Lambda \sim \rho d^3 = O(1)$ (see Ref. 8 for a more detailed discussion). Thus the diluteness assumption necessary for the validity of the cascade/Boltzmann equation approaches is not justified and one must consider microscopic approaches which do not depend on this assumption.

C. The classical-equations-of-motion (CEOM) approach[2-5]

This is then the only available microscopic approach which includes interaction effects for realistic potentials and hence does not assume a dilute fluid. This approach is essentially the molecular dynamics approach which has been so fruitful for the understanding of classical liquids. It assumes the validity of a classical description (i.e., "$h \approx 0$"), which is perhaps not unreasonable at energies $\gtrsim$300–500 MeV/nucleon,[8] but even then cannot be fully justified.

Thus unfortunately there seems to be no completely justified simplification for HE-HI collisions and in principle a complete A-body quantum mechanical description (or even relativistic quantum field theory description) is required. Since this is not feasible one is perforce limited to the three *a priori* but approximate approaches. As indicated, these involve different distinct approximations and are to some extent complementary, each one having its own unique features. For a satisfactory understanding of HE-HI collisions it will be necessary to make rather comprehensive and definitive studies with each approach.

The unique features of the CEOM approach are that it is a completely microscopic, albeit classical description, and thus capable of describing arbitrarily large nonequilibrium and transparency effects, while at the same time including finite-range interaction effects. In particular it is capable of describing nontrivial (non-ideal gas) equation-of-state effects as well as finite-range interaction effects on dissipation. Also, since it is a fully microscopic approach, it is capable, in principle, of describing–classically–any correlations including perhaps some estimates of cross sections for the production of composites.

The present CEOM calculations are nonrelativistic and have made for laboratory energies of $E_L/A_P \leq 800$ MeV and for the symmetric collisions $A_P = A_T = 20$ (Ne+Ne) and $A_P = A_T = 40$ (Ca+Ca). Pion production, the distinction between neutrons and protons, spin, and Coulomb interactions have been neglected. The neglect of the difference between neutrons and protons and neglect of Coulomb interactions at high energies seems justified for the fairly small mass numbers $A_P, A_T \leq 40$ which we have considered. Relativistic corrections to order v^2/c^2 can be calculated and some preliminary calculations have been made for individual configurations.[8,13] However, so far no calculations to order

v^2/c^2 have been made for a complete ensemble of initial configurations. Earlier nonrelativistic CEOM calculations were reported in Ref. 2 and some preliminary results of the present calculations in Ref. 9.

II. CLASSICAL-EQUATIONS-OF-MOTION CALCULATIONS

Our version of the CEOM approach has been described previously,[2] and our implementation of the CEOM calculations is therefore only briefly described here. A somewhat different implementation of the CEOM approach has been made by Wilets and co-workers[3] who include a momentum dependent Pauli potential in their interaction. Classical trajectory calculations with hard sphere interactions have been made by Halbert *et al.* and also by Noack *et al.*[4] Also, more recently, CEOM calculations have been made by Sano and coworkers.[5]

Implementation of the CEOM approach involves four elements:

1. Construction of a two-body potential.
2. Choice of an ensemble of initial configurations of positions and momenta $\vec{x}_i, \vec{p}_i$ ($i=1,\ldots,A_P$ for the projectile, $i=A_P+1,\ldots,A$ for the target) representing the initial nuclei.
3. A-body trajectory calculations for each initial configuration.
4. Analysis of the trajectory data and averaging over the initial ensemble.

These elements are now described in more detail.

1. Two-body potentials

These are chosen to satisfy the following requirements:

(a) To be physically reasonable; thus our static potential $V_{st}(r)$, described below, is required to have a reasonable repulsive core and attractive tail.

(b) To fit certain aspects of the NN scattering data, namely the average $np+pp$ cross section $\sigma^{(2)}$ (see Refs. 2, 8 for empirical values) for a reasonable range of energies with use of *classical* two-body calculations. Here $\sigma^{(n)}=2\pi\int\sigma(\theta)(1-\cos^n\theta)\times d(\cos\theta)$ and $\sigma(\theta)$ is the c.m. differential cross section. Because of diffraction and exchange effects, one cannot fit the complete cross section $\sigma(\theta)$ with a classical trajectory calculation using a static potential. We have chosen to fit $\sigma^{(2)}$ because this determines the viscosity and thermal conductivity in a Boltzmann equation approach for conditions close to equilibrium, and these transport coefficients in turn determine the dissipation, and in particular shock structure, for the hydrodynamic (Navier-Stokes) equation. In fact, it is not even possible classically, with a static potential, to obtain good fits for both $\sigma^{(1)}$ and $\sigma^{(2)}$, where $\sigma^{(1)}$ is the longitudinal momentum loss cross section.[14] Thus our potentials, which have been fitted to $\sigma^{(2)}$, give too small values for $\sigma^{(1)}$.[8]

(c) To give a reasonable binding energy ($\approx$8 MeV/nucleon) for the initial nuclei. With an average internal kinetic energy/nucleon of $\overline{T}\approx 20$ MeV (see below), this implies that the potentials are required to give an average potential energy of ≈ -28 MeV/nucleon.

Our best static potential, fitted to the above requirements, and of the form

$$V_{st}(r)=V_R r^{-1}\exp(-\mu_R r)-V_A r^{-1}\exp(-\mu_A r) \quad (1)$$

is then obtained for $V_A=2569$ MeV fm, $\mu_A=2.469$ fm^{-1}, $V_R=6569$ MeV fm, $\mu_R=3.358$ fm^{-1}. [The minimum is at 1.32 fm with a value of -17 MeV; also $V_{st}(0.67\text{ fm})=300$ MeV, $V_{st}(0.81\text{ fm})=100$ MeV, and $V_{st}(1.05\text{ fm})=0$.] This static potential was used for the present calculations and is slightly different from that of Ref. 2.

In addition to V_{st} we also used a scattering equivalent "transformed" potential V_{tr} which is momentum dependent and which is discussed below in Sec. III.

2. Initial configurations

An ensemble of N initial configurations is chosen to represent the initial projectile and target nuclei with a relative velocity appropriate to the laboratory energy E_L and impact parameter b. The projectile (target) configurations of $A_P(A_T)$ positions and momenta have been chosen to have approximately the desired nuclear radius, a uniform (Fermi) distribution of momenta corresponding to a reasonable average kinetic energy $\overline{T}$ ($\approx$20 MeV/nucleon), short-range correlations appropriate to the repulsive core of the two-body potential, and reasonable binding energies determined from the kinetic and potential energies (see above). These configurations do not saturate at normal densities and are hot. Thus they condense and evaporate. This is not too serious on the time scale of the nuclear collisions for the light equal-mass nuclei ($A_P=A_T=20,40$) which we have considered, and is minimized by starting the initial projectile and target configurations as close to each other as is consistent with a negligible potential energy of mutual interaction. However, these features are clearly undesirable and restrict the present range of applicability of the calculations. The size of the ensembles used was $N=32$ and 21 for $A_P=A_T=20$ and 40, respectively. These values of N were chosen as a compromise between the needs for adequate

statistics and reasonable computing times for the trajectory calculations.

Since the CEOM approach is completely microscopic, a collision for a given initial configuration, representing the projectile and target nuclei, is the computer analog of a collision of a single projectile nucleus with a single target nucleus—for a specified impact parameter b. Thus an ensemble of N initial configurations corresponds to N collisions. The rather small values of N which we used suffice to give generally adequate statistics for single-particle inclusive cross sections but are too small, by an order of magnitude at least, to give adequate statistics for two-particle correlations.[15]

3. *A-body dynamical trajectory calculations*

These are made (for a given impact parameter b and laboratory energy E_L) for each initial configuration of the ensemble and are continued until the collision is effectively over. The calculations of Ref. 2 were made using Newton's equations. The present calculations use Hamilton's equations which must be used for relativistic calculations [with the Hamiltonian to $O(v^2/c^2)$ given by Eqs. (8)–(10)] or for nonrelativistic calculations with momentum dependent potentials such as the transformed potential. The accuracy of the trajectory calculations is monitored by checking the conserved quantities throughout the calculation; checks have also been made by calculation of the time reversed A-body trajectories.[8]

Most of the computing time comes from the trajectory calculations and it is these that in practice limit the ensemble size N.[16]

4. *Analysis of trajectories*

The information from the trajectory calculations (transferred to magnetic tape) is analyzed by appropriate binning, to give physically interesting quantities and the results are then averaged over the ensemble of configurations. The analysis is straightforward in principle but involves extensive programs involving a large number of physical quantities which can be obtained at any desired time during a collision. For inclusive cross sections an integration over impact parameter must finally be made.[16]

III. SCATTERING EQUIVALENT ("TRANSFORMED") POTENTIALS

Monahan *et al.*[17] have shown that by use of canonical transformations which asymptotically preserve the scale one can obtain from a given (e.g., a static) potential other (momentum dependent) "transformed" potentials which give the identical asymptotic two-body trajectories (same deflection function) and therefore the identical two-body scattering as the original potential. Such scattering equivalent potentials will not of course give the same two-body trajectories for small separations. Also when dense conditions occur for which three or more nucleons interact simultaneously such scattering equivalent potentials will not give the same A-body scattering. In effect they will be associated with different equations of state and with different transport properties, although for dilute conditions, for which the Boltzmann equation is applicable, they would give the same results (the same–i.e., ideal gas–equation of state, and the same transport coefficients since the collision term, which depends only on $\sigma^{(2)}$, is the same). Thus use of scattering equivalent potentials allows study for HE-HI collisions of finite-range interaction effects, in particular of equation-of-state related effects, especially for dense conditions expected for central or near central collisions.

The two-body canonical transformation is of the general form

$$r' = f(r) \quad \text{with } f(r) \to r \quad \text{as } r \to \infty .$$

The requirement $f(r) \sim r$ ensures that asymptotically the two-body trajectories are the same for the original and for the transformed potential. The latter is easily obtained and for a static potential $V_{st}(r)$ is

$$V_{tr}(r, p_r, l) = V_{st}(f(r)) + V_p(r, p_r, l), \tag{2}$$

with

$$V_p(r, p_r, l) = \frac{1 - f'^2}{f'^2} p_r^2 + \frac{r^2 - f^2}{f^2} \frac{l^2}{r^2}, \tag{3}$$

where $f' = df/dr$, l is the angular momentum, and $p_r = \vec{p} \cdot \vec{r}/r$ is the radial momentum conjugate to r.[17] Instead of l one can use the relative momentum p by use of $p^2 = p_r^2 + l^2/r^2$. Thus V_{tr} depends on both possible relative momenta p_r and l, and is a momentum dependent potential of the most general type. The potential $V_p(r, p_r, l)$ gives no scattering, i.e., the (asymptotic) deflection function is identically zero, since it is the scattering equivalent potential for an identically zero potential. Of course for small r, V_p gives nonzero deflection.

Trajectory calculations (both two- and A-body) with V_{tr} must use Hamilton's equations since the potentials are momentum dependent. Two-body trajectory calculations made for V_{tr} of course verify that the deflection function, and hence also the cross sections and in particular $\sigma^{(2)}$, are the same as for V_{st}. An example of a two-body trajectory [with the $f(r)$ given below] illustrating the above features is shown in Fig. 1.

The transformation actually used is

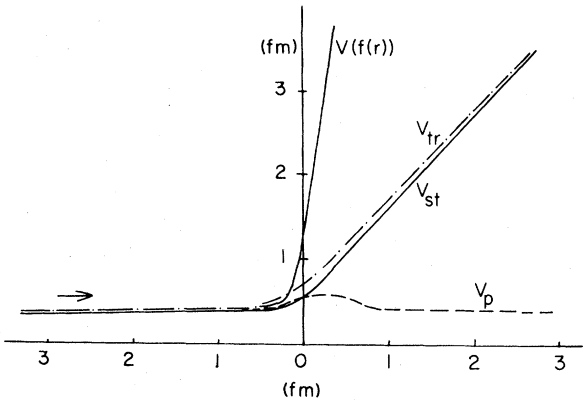

FIG. 1. Projectile trajectories for two-body scattering in the c.m. system for $E_L = 300$ MeV, $b = 0.8$ fm, and for V_{st} and $V_{tr} = V(f(r)) + V_p$; V_p is the momentum dependent, zero-scattering part of V_{tr}.

$$f(r) = r(1 - e^{-\mu r}). \tag{4}$$

The value $\mu = 1.88$ fm^{-1} gives a V_{tr} which also gives the same average potential energy/nucleon ≈ -28 MeV, and hence the same binding energy as V_{st} for the ensemble of initial nuclei with $A_P = A_T = 20$. Scattering equivalent potentials do not of course in general give the same potential energy for identical configurations. No calculations with V_{tr} have been made for $A_P = A_T = 40$.

IV. "COLLISIONS" AND AVERAGE POTENTIAL—A NEW KINETIC EQUATION DESCRIPTION

In this and the following section we discuss some guiding physical considerations for HE-HI collisions, with emphasis on central collisions. These considerations will also be helpful in the subsequent discussion of our CEOM results.

The CEOM approach uses finite-range two-body potentials; hence except for quite dilute conditions (e.g., $\rho \lesssim 0.5\rho_0$), it is not very meaningful to refer to a mean free path or to single, double, etc. collisions for the complete two-body potential since this has a range of about 1.5 fm. However, the following plausible description, which was suggested by our results, still allows one to talk about "collisions" and a mean-free path. This description is represented by a kinetic equation for the one-body distribution function $f(\vec{x}, \vec{p}, t)$. It depends on being able to make a significant distinction, in particular for the time scales, between the physical effects associated with the strong short-range and the weak long-range parts of the two-body potential. The potential is thus separated, at a distance d, into two parts:

$$V = V_{\text{short}} + V_{\text{long}}, \tag{5}$$

The kinetic equation is then (for a static two-body potential)

$$\frac{\partial f}{\partial t} + \frac{\vec{p}}{m} \cdot \nabla_{\vec{x}} f + \vec{F}(x) \cdot \nabla_{\vec{p}} f = \left(\frac{\partial f}{\partial t}\right)_{\text{coll}}, \tag{6}$$

where

$$\vec{F}(\vec{x}) = -\vec{\nabla}\overline{V}(\vec{x}),$$
$$\overline{V}(\vec{x}) = \int V_{\text{long}}(|\vec{x} - \vec{x}'|)\rho(\vec{x}')d^3\vec{x}'. \tag{7}$$

V_{short} is identified with the short-range part of the potential; i.e., effectively, mainly the repulsive part of the potential. Thus a natural choice would be $d = d_0$, where $V(d_0) = 0$ (i.e., V_{short} is just all the positive part of the potential; for V_{st}, $d_0 \approx 1.0$ fm). In any case V_{short} is assumed to give rise to rapidly fluctuating forces and high momentum components, i.e., to collisions, and is the part of the potential used for the collision term $(\partial f/\partial t)_{\text{coll}}$. If V_{short} is plausibly replaced by an effective infinite hard core (of radius $\approx d$), then $(\partial f/\partial t)_{\text{coll}}$ will be the Enskog collision term appropriate to hard spheres;[12] this includes finite-range and potential energy effects through excluded volume terms which are absent in the Boltzmann collision term. Thus for V_{short} it is reasonable to speak about single, double, and in general multiple collisions, about a mean-free path, and about the number of nucleon-nucleon collisions which have occurred up to some time. Since collisions are due to V_{short} only, the corresponding differential scattering cross section $\sigma_{\text{short}}(\theta)$, relevant for $(\partial f/\partial t)_{\text{coll}}$, is much more isotropic than the complete cross section $\sigma(\theta)$ and in particular does not have the pronounced forward peak of the latter.

The long-range part of the potential V_{long} is assumed—for not too dilute conditions—to give much more smoothly varying forces and much lower momentum components than V_{short}. Correspondingly, its effect, for not too dilute conditions, is assumed to be through the average single-particle potential $\overline{V}$ (folding potential due to V_{long}). Without the collision term [i.e., with $(\partial f/\partial t)_{\text{coll}} = 0$] one would just have a nuclear analog of the Vlasov equation for which changes of f due to the interactions occur only through the average field $\overline{V}$. Finite-range interaction effects are thus included both through the collision term, involving V_{short}, and through the average potential $\overline{V}$, involving V_{long}. [Cascade calculations which have included an average single-particle potential[18] seem in effect equivalent to a Boltzmann equation of the above form where, however, the collision term is the usual Boltzmann term involving the free cross section $\sigma(\theta)$, and where $\overline{V}$ is an average single-particle potential with the implicit assumption that this is the result

of the *complete* two-body potential. Such an approach seems unjustified not only because of the "double counting" of the interaction in both $\bar{V}$ and $(\partial f/\partial t)_{\text{coll}}$, but also because the short time scale of the collisions necessary for the validity of the Boltzmann term is inconsistent with the long time scale required for the use of $\bar{V}$.]

The main agent responsible for equilibration is expected to be $(\partial f/\partial t)_{\text{coll}}$, i.e., the collisions due to V_{short}. Such collisions will give real equilibration, leading to a Maxwell-Boltzmann distribution. However, time variations of $\bar{V}$, due to changes in ρ, can also give dissipation and pseudo-equilibration through "particle-wall" collisions. (Thus rapid changes of $\bar{V}$ may give quite effective "stirring" of the trajectories in the six dimensional one-body phase space, and hence to a pseudo-equilibrium as for the Vlasov equation.) The effect of $\bar{V}$ is expected to lead to fragmentation-type effects even for central collisions, but not to the more complete thermalization expected for central collisions.

An important extension of the above description is to allow the separation distance d to depend on the density ρ, increasing as ρ decreases such that $d \to \infty$ as $\rho \to 0$. For a dilute system one then recovers the Boltzmann equation since $\bar{V} = 0$, and the complete two-body interaction is then included in the collision term of the Boltzmann form [which depends on the interaction only through the free cross section $\sigma(\theta)$]. Dilute conditions for which such an extension is required are expected to occur for peripheral collisions or for the initial or late expansion stages of central collisions.

In summary, the above kinetic-equation description depends on the justifiability of separating the two-body potential—for not too dilute conditions—into a strong short-range repulsive part and a weak longer-range attractive part, with the former giving collisions and the latter an average single-particle potential. Thus the picture is one of collisions (due to V_{short}) occurring in a background average single-particle potential $\bar{V}$ (due to V_{long}). When we subsequently refer to single, double, etc. collisions or to a mean-free path, we then imply that these are to be associated with V_{short}.

The above description is, in effect, a simplification of the more general CEOM approach, but one which does include finite-range effects of both the short- and long-range parts of the interaction. It thus contains considerably more physics than presently used Boltzmann-type equations or the related cascade calculations.[12] It also offers the possibility of including exclusion-principle (blocking) effects through final state factors in the collision term, as for the Boltzmann equation. Pion production might be included on the lines of current cascade calculations.[11] The computational implementation of the kinetic equation could be through suitable modifications of the CEOM calculations (see also Sec. XI).

Potential energy effects. For central or near central collisions and when conditions are close to that of maximum density, the potential energy may become quite large and negative (for our two-body potentials), whereas in the late stages of the expansion the potential energy generally becomes quite small, since for small impact parameters the nucleons are then mostly well separated from each other (little clustering). Thus there must be a corresponding decrease in kinetic energy between the beginning and end of the expansion as a result of the work needed to separate the nucleons from each other. Study of the momentum distribution (i.e., of $d^3\sigma/dp^3$), results for which are extensively discussed below, gives detailed insight into how this decrease in kinetic energy is distributed in momentum space and what the relevant role of the interactions is.

We again emphasize that potential-energy effects, and more generally finite-range effects, can only be studied with the CEOM approach or a kinetic-equation approach which includes such effects. To date the CEOM approach is the only microscopic approach which has been used for HE-HI collisions, which includes finite-range effects and therefore nontrivial equation-of-state effects. To more clearly identify such effects we present results obtained both with the static potential V_{st} and with the scattering equivalent transformed potential V_{tr}.

V. SINGLE AND MULTIPLE COLLISIONS; COLLECTIVE EFFECTS

Single, double, etc. *NN* collisions are understood to be due to V_{short}, which, however, may vary during a nucleus-nucleus collision as discussed above.

The initial c.m. momentum distribution (region *I* in Fig. 2) corresponds to the projectile and target c.m. momentum (per nucleon), of magnitude $p_{\text{c.m.}} = (mE_L/2)^{1/2}$, as modified by the internal (Fermi) momentum distributions (of radius p_F). Figure 2 is the same for all impact parameters.

Single *NN* collisions between projectile and target nucleons (in I_P and I_T, respectively) will, consistent with energy and momentum conservation (and neglecting for the moment any possible effects of V_{long} via $\bar{V}$)— i.e., by quasifree scattering—populate region *II* with an angular distribution determined by V_{short}, where the latter may, however, be effectively quite close to V especially for the early initial stage and for peripheral collisions. For $A_P = A_T$ there will be symmetry about a plane through the origin and perpendicular to the beam

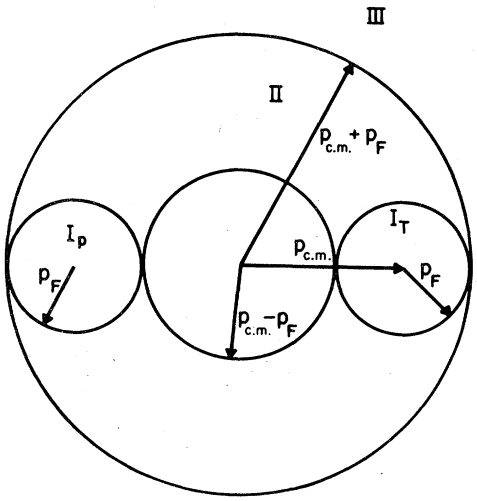

FIG. 2. Momentum space regions for collisions of equal mass projectile and target. I_P denotes the initial momentum region for the projectile and I_T that for the target. The scale corresponds to $E_L = 800$ MeV, $E_F \approx 33$ MeV.

direction, and the range of accessible momenta, corresponding to region *II*, will be $p_- = p_{c.m.} - p_F \leq p \leq p_+ = p_{c.m.} + p_F$. [The corresponding limiting energies are $E_\pm = E_L/4 + E_F \pm (E_L E_F)^{1/2}$.] Single *NN* collisions (quasielastic scattering) are expected to dominate peripheral (nucleus-nucleus) collisions or the initial stage of central collisions when the population in *II* (outside *I*) is relatively small. Such conditions, appropriate to dominance of the relatively slightly depleted initial distribution in *I*, correspond to large transparency, with an expected momentum distribution similar to that of peripheral, or fragmentation, collisions for which the distributions are strong forward peaked and do not differ too much from the initial distribution.

As the population of singly scattered nucleons in *II* builds up, these nucleons will begin to scatter with each other and with the nucleons in *I*, i.e., multiple scattering will occur. In particular, multiple scattering is first expected to occur predominantly between a (quasielastically scattered) nucleon in *II*, particularly one in the more populated forward directions, and a nucleon in the initial region *I*, since the nucleons in *I* still dominate due to their relatively small depletion. As multiple and further single *NN* collisions occur, the momentum distribution is expected to become more isotropically populated because of multiple scattering and also because V_{short} for the relevant dense conditions will be quite similar in its effects to a purely repulsive core, and a possible eventual approach to a thermalized, i.e., to a Maxwell-Boltzmann distribution may occur. A more detailed discussion along the above lines is given by Randrup *et al.*[19] We recall that considerations based on simplified cascade or Boltzmann-equation calculations[20] indicate that roughly three collisions suffice for attainment of equilibrium.

In the early stages of the final expansion stage of central collisions the density is still quite large and collisions due to V_{short} are expected to be quite effective in leading to equilibrium, i.e., in giving dissipation. In the later stages, when conditions are more dilute, V_{short} will approximate more closely to the complete potential and dissipative effects are expected to be smaller. Eventually for small enough densities (such that the mean separation between nucleons becomes significantly larger than the mean-free path) scattering will effectively cease and the expansion will be that of a free ideal nucleon gas.

Collective and hydrodynamic behavior. This may be expected to occur when there is approximate local equilibrium as a result of *NN* scattering, especially multiple scattering. Consistent with the description discussed above, hydrodynamic effects may occur in a background single-particle potential $\overline{V}$ due to V_{long}. In particular, we shall be interested in hydrodynamic-type behavior for the expansion stage of central collisions. The following are effects we have looked for, in addition to dissipation, during the expansion.

1. Development of transverse peaking of the angular distribution during the expansion, i.e., development of a density distribution which is compressed in the beam direction and of a (c.m.) momentum distribution which is larger perpendicular to the beam than along it.[21]

2. Conversion of internal energy (temperature) into collective (radial) motion as a result of gradients of the density and pressure in the "fireball" which results from the stages of the collision prior to the expansion stage: the "blast wave" model of Siemens and Rasmussen.[22] Such conversion might be expected if approximate (local but of course not global) equilibrium has developed and if the expansion is approximately isentropic. Thus, as the expansion proceeds, the collective radial velocity may increase at the expense of the internal energy, leading to a cooling in the local frame of reference at rest with respect to the collective motion. A peak in the momentum distribution will then be expected at any energy corresponding to the radial velocity of expansion, and this peak is then expected to move to *higher* energies with some concurrent increase in (negative) slope of the tail of the distribution above the peak as the expansion proceeds. Conversion of internal into collective energy will cease when the density becomes so low that the mean-free path has become sufficiently

large that nucleon-nucleon collisions effectively cease.

VI. RESULTS OF CEOM CALCULATIONS (Ne + Ne,Ca + Ca)

For $A_P = A_T = 20$ (Ne + Ne) we present results for both the static and transformed potentials V_{st} and V_{tr}; for $A_P = A_T = 40$ (Ca + Ca) we have results only for V_{st}.

Results are presented for a number of quantities, in particular for the momentum space distribution $d^3\sigma/dp^3$ which for $b = 0$ is shown as a function of time. At any particular time during the collision this distribution is proportional to the (asymptotic) c.m. double differential inclusive nucleon cross section if the interactions were switched off for later times, with the nucleons then propagating freely to infinity. Thus

$$\frac{1}{p}\frac{d^2\sigma}{dE\,d\Omega} = \frac{m}{p^2}\frac{d^2\sigma}{dp\,d\Omega} \equiv m\frac{d^3\sigma}{dp^3},$$

where p and E are the nucleon momentum and energy, respectively. We show results for this ("invariant") cross section (for $b = 0$ as a function of time) which is then nonrelativistically just the corresponding momentum space distribution. Only for late times is this to be identified with the actual asymptotic (observable) cross section. The time development of $d^3\sigma/dp^3$ thus gives a rather detailed picture of the evolution of a collision. [Of course a more complete picture would be given by the one-body distribution function $f(\vec{x}, \vec{p}, t)$, i.e., the density in the six-dimensional one-body phase space.]

For $A_P = A_T$ the momentum distribution in the c.m. system is symmetrical with respect to the plane perpendicular to the beam direction and through the origin. We thus show only the results for the forward hemisphere $p_z \geq 0$. In fact, to obtain improved statistics the results are an average over the corresponding forward and backward directions. The cross sections are, for $A/2$ nucleons, appropriate to results for only protons. Details of the energy and $\cos\theta$ bins are given in the captions of Figs. 9, 17, and 25.[23]

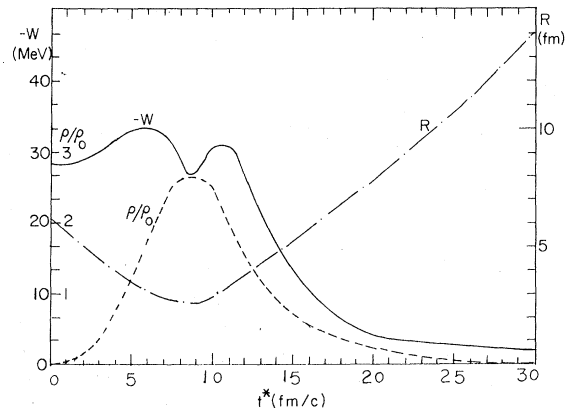

FIG. 3. Potential energy/nucleon $-W$, equivalent uniform rms radius R, and density ratio ρ/ρ_0 vs reduced time t^* for $b = 0$, $A_P = A_T = 20$, $E_L = 800$ MeV ($t^* = 1.41\,t$) and for V_{st}.

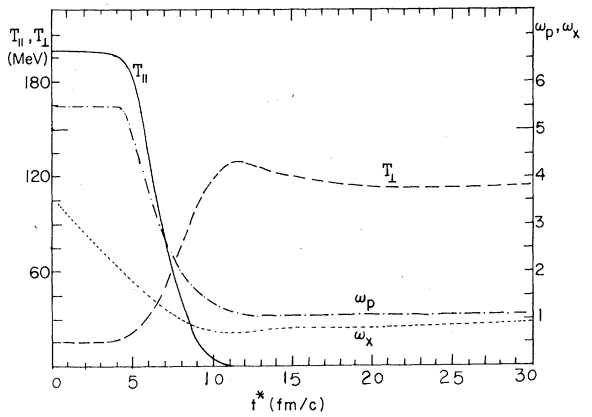

FIG. 4. Kinetic energy/nucleon in c.m. system in beam direction $T_\parallel$, transverse kinetic energy/nucleon $T_\perp$, c.m. momentum asymmetry ω_p, and position asymmetry ω_x vs t^* for $b = 0$, $A_P = A_T = 20$, $E_L = 800$ MeV and for V_{st}.

We also discuss results for the following quantities: $\omega_p = \langle p_z^2/\frac{1}{2}(p_x^2 + p_y^2)\rangle^{1/2}$ (momentum asymmetry), $\omega_x = \langle z^2/\frac{1}{2}(x^2 + y^2)\rangle^{1/2}$ (position asymmetry), $-W$ (potential energy/nucleon), $R = \frac{5}{3}\langle r^2\rangle^{1/2}$ (radius of uniform distribution with same rms value as the position distribution); ρ/ρ_0 (ratio of average density inside sphere of radius 2 fm with center at c.m. to initial average density $\rho_0 = 0.23$ fm^{-3}); $T_\perp$ (component of average kinetic energy/nucleon perpendicular to beam); Y/Y_0 (ratio of average rapidity of projectile nucleons to initial rapidity = $-$ratio for target nucleons); $T_\parallel = Y^2/2A_P m$ (beam kinetic ener-

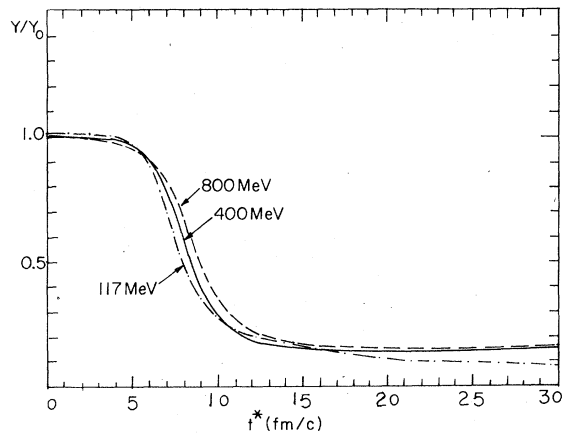

FIG. 5. Y/Y_0 vs t^* for the indicated energies. Y is the rapidity for the projectile (or target) nucleons. Y_0 is the initial value (0.65c, 0.46c, 0.25c for $E_L = 800$, 400, and 117 MeV). The results are for $b = 0$, $A_P = A_T = 20$ and V_{st}.

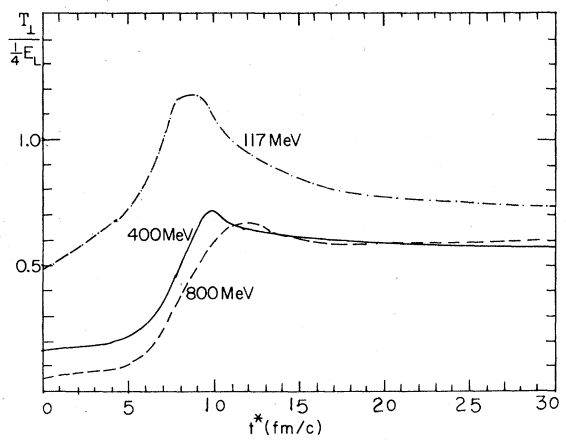

FIG. 6. Relative transverse kinetic energy/nucleon $T_\perp/\frac{1}{4}E_L$ vs t^* for the indicated energies and for $b=0$, $A_P=A_T=0$, and V_{st}.

gy/nucleon of projectile or target nucleons). These quantities are given in the captions for the figures showing $d^3\sigma/dp^3$ and are also shown in Figs. 3–8.

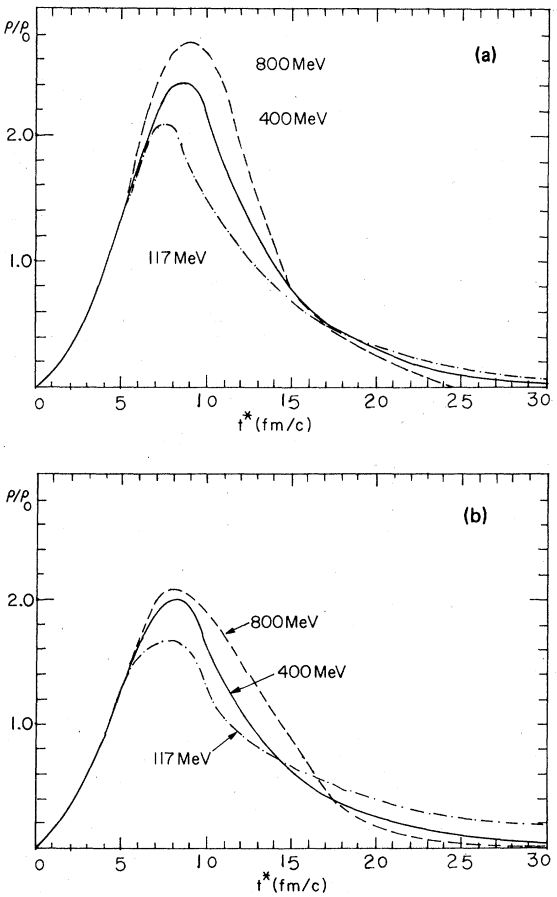

FIG. 7. ρ/ρ_0 vs t^* for the indicated energies for $b=0$, $A_P=A_T=20$, and (a) V_{st} and (b) V_{tr}.

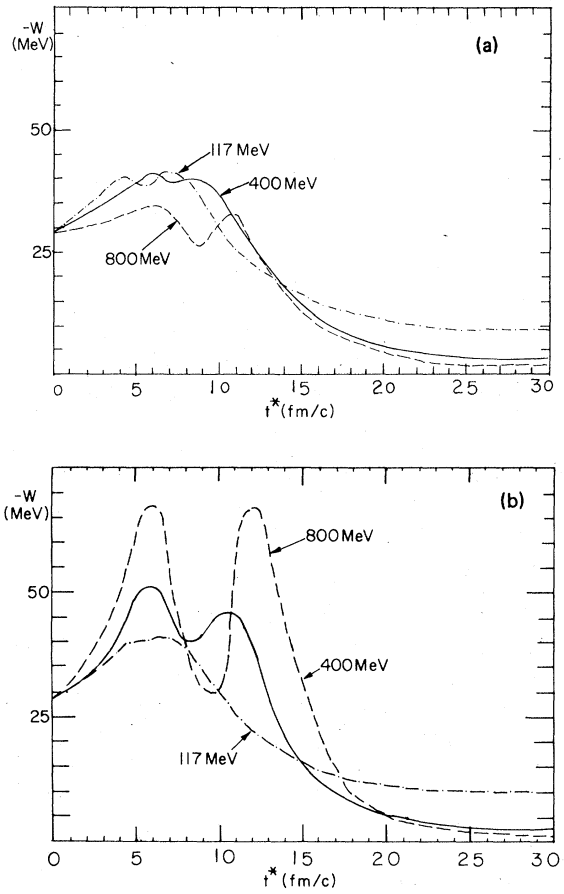

FIG. 8. Potential energy/nucleon $-W$ vs t^* for the energies indicated and for $b=0$, $A_P=A_T=20$, and (a) V_{st} and (b) V_{tr}.

It is helpful to consider the evolution in terms of a reduced time t^* which is t scaled with the c.m. velocity. We normalize t^* to $E_L=400$ MeV; thus $t^*=(E_L/400)^{1/2}t$; in particular $t^*=\sqrt{2}t$ for $E_L=800$ MeV. If there were no mutual interaction between projectile and target then, for example, ρ/ρ_0 and Y/Y_0 would be the same function of t^* for all energies.

VII. CENTRAL COLLISIONS

A. General features

On the basis of our results we can distinguish three distinct stages in the evolution of a central (or near central) collision: (1) an initial, transparent stage which lasts until about maximum overlap, i.e., for $t^* \lesssim 7$ fm/c ($t \lesssim 5.5$ fm/c for 800 MeV), (2) a strong interaction (multiple scattering) stage for $7 \lesssim t^* \lesssim 12$ fm/c ($5.5 \lesssim t \lesssim 8$ fm/c for 800 MeV), and (3) an expansion stage (when $\rho \lesssim \rho_0$ and $R \gtrsim 4$ fm) for $t^* \gtrsim 12$ fm/c ($\rho/\rho_0 \lesssim 0.2$, $R \gtrsim 8$ fm for

$t^* \gtrsim 20$ fm/c). The times are approximate, there being no sharp dividing line between successive stages. As a function of t^* the evolution is more rapid for lower E_L, consistent with a large cross section $\sigma^{(2)}$ and a correspondingly shorter mean-free path Λ, and hence more dissipation.

Figures 3 and 4 for $A_P = A_T = 20$, $E_L = 800$ MeV illustrate some general features of the evolution for $b = 0$. Figures 5–8 compare various quantities vs t^* at different energies E_L for $A_P = A_T = 20$. For V_{tr} results are only shown for ρ (Fig. 7) and W (Fig. 8), since the other quantities are quite similar to those for V_{st}.

Y/Y_0, and hence also the beam kinetic energy $T_\parallel$, decrease rapidly during an interval of t^* of about 4–5 fm/c, consistent with $\Lambda \approx 2$ fm. The dependence of Y/Y_0 is approximately the same for the energies considered, corresponding to approximate scaling of Y/Y_0 (Fig. 5). The slightly more rapid falloff for lower E_L is consistent with more rapid dissipation. Also dissipation is somewhat greater for $A_P = A_T = 40$. The final values of Y are quite small corresponding to dissipation of most of the initial beam momentum and consistent with approximate final isotropy ($\omega_p \approx 1$). Y/Y_0 is for the most part quite similar for V_{st} and V_{tr}. A slight initial increase in Y/Y_0 for V_{tr} can be understood as due to an increasingly attractive potential energy $-W$ at early times which leads to a corresponding increase Y and $T_\parallel$ before dissipation sets in strongly for $t^* \gtrsim 5$ fm/c.

The momentum isotropy ω_p (Fig. 4) decreases rapidly from its initial value, more or less in step with Y/Y_0, and at the end of the second stage is generally already fairly close to its final value. However, this is not true for the position distribution which is still quite compressed in the beam direction; thus ω_x only approaches ω_p later during the collision. For $A_P = A_T = 40$, the momentum distribution becomes transversely peaked ($\omega_p < 1$) during the expansion phase, as discussed in more detail below.

The transverse kinetic energy $T_\perp$ (Fig. 6) attains a maximum at approximately what is considered the beginning of the expansion stage. For $E_L \gg \overline{T} \approx 20$ MeV (initial internal kinetic energy), there may perhaps be approximate scaling of $T_\perp/E_L$ as a function of t^*. Because of the contribution due to $\overline{T}$ there cannot, however, be even approximate scaling for lower E_L. Thus the relatively large initial value [$T_\perp(t=0) \approx \frac{2}{3}\overline{T} \approx 13$ MeV] presumably accounts for the much larger peak in $T_\perp/(\frac{1}{4}E_L)$ vs t^* for $E_L = 117$ MeV than for the larger values of E_L. The contribution of the internal energy to $T_\perp$ is also consistent with a somewhat larger peak for $E_L = 400$ than for $E_L = 800$ MeV. The earlier occurrence of the peak for lower E_L is again consistent with more rapid dissipation at lower E_L.

The slow decrease in $T_\perp$ at later t^* is consistent with increasing potential energy (Fig. 8). Thus, as the density decreases during the expansion, the nucleons become increasingly separated from each other. The work needed for this is at the expense of the kinetic energy which thus decreases during the expansion.

The density ρ/ρ_0 vs t^* (Fig. 7) shows a common increase for all energies up to $t^* \approx 5$ fm/c. The interpretation of this is that during the early stage of a collision the projectile and target pass through each other only slightly changed by their mutual interaction, corresponding to initially very transparent conditions, ρ attains a maximum (and R correspondingly a minimum) for $t^* \approx 7$–9 fm/c.

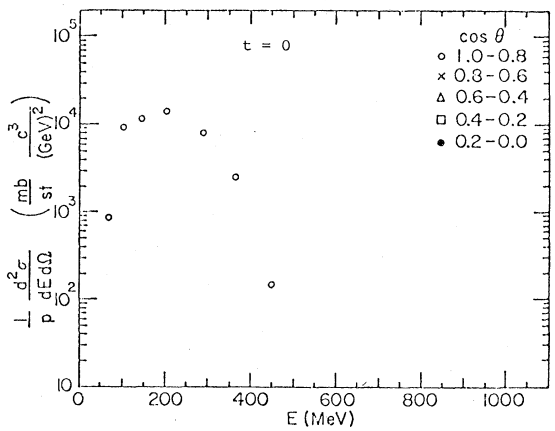

FIG. 9. "Invariant" c.m. inclusive double differential cross section (momentum distribution) at $t = 0$ fm/c for $A_P = A_T = 20$, $E_L = 800$ MeV. The distribution shown in this and all following figures are the invariant ones for protons in the c.m. system. The initial distribution shown in this figure is the same for all impact parameters. $\Delta z = 0$ fm (Δz is the displacement relative to $t = 0$ of c.m. of projectile nucleons = −displacement of c.m. of target nucleons). $R = 6.03$ fm (equivalent uniform rms radius). $\rho/\rho_0 = 0$ (ρ is the average density in sphere of radius 2 fm with origin at c.m.; $\rho_0 = 0.23$ fm^{-3}). $\omega_p = 5.54$ (momentum asymmetry). $\omega_x = 3.61$ (position asymmetry). $W = 28.1$ MeV (magnitude of potential energy/nucleon). $T_\perp = 13.4$ MeV (transverse kinetic energy/nucleon). $Y/Y_0 = 1$ [Y is the magnitude of the rapidity for projectile or target nucleons; $Y_0 = Y\,(t=0)$]. The values shown in this and the following figures (Figs. 10–16) for $E_L = 800$ MeV are for the indicated cos θ bins (of size 0.2). The energy bins are of size $\Delta E = 40$ MeV for $E < 200$ MeV and $\Delta E = 80$ MeV for $E \geq 200$ MeV. The values are plotted at the center of the appropriate energy intervals. Also given in the captions are values of the peak energy E_p when an approximately common peak has formed and of the temperature θ of the distribution in the region above the peak, again when appropriate. The values of E_p and θ are approximate. Figures 9–32 are for a central collision: $b = 0$.

The maximum value of ρ/ρ_0 is somewhat more than two for V_{st} and increase with E_L; for V_{tr} the maximum value is about two or slightly smaller and again increases with E_L. It is perhaps reasonable that ρ_{max} is larger for larger E_L, since with higher kinetic energies the nucleons can approach closer to each other, against the repulsive core of the two-body potential. This is consistent with the increasingly pronounced dip in the *negative* potential energy $-W$ (Fig. 8) as E_L increases. The minimum of this dip in fact occurs at a time close to that of the corresponding maximum in ρ. A larger ρ is then associated with a smaller average attractive potential energy since the nucleons are then on the average closer to each other and feel the repulsive core more strongly.

The somewhat larger values of ρ/ρ_0 for V_{st} [Fig. 7(a)] than for V_{tr} [Fig. 7(b)] are, similarly, plausibly related to the larger dip of $-W$ for V_{tr} than for V_{st} near conditions of ρ_{max}. Thus more repulsive potential energy for V_{tr} is a reflection of more repulsive, short-range, two-body interactions (than for V_{st}) which would tend to keep the nucleons further apart for V_{tr}, corresponding to lower densities.

The pronounced double humped shape of W vs t^* for V_{tr} [Fig. 8(b)] seems characteristic of momentum dependent potentials (including relativistic retarded potentials) and seems associated with the transition from motion along the beam direction to an approximately isotropic expansion. The first

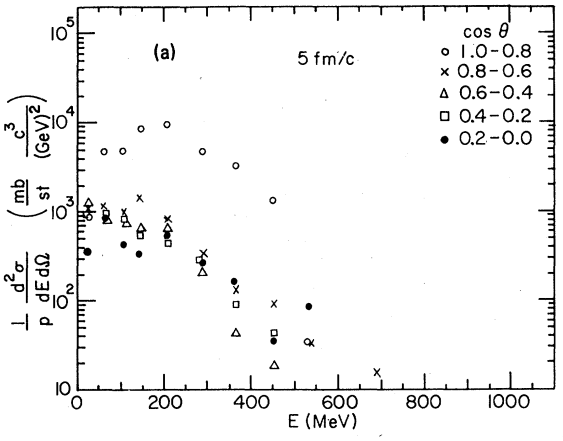

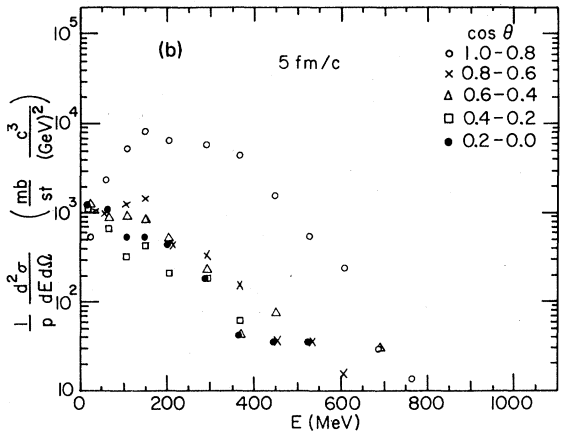

FIG. 10. As for Fig. 9. Results at $t=5$ fm/c. For (a) V_{st}: $\Delta z=3.16$ fm, $R=2.84$ fm, $\rho/\rho_0=2.39$, $\omega_\rho=2.71$, $\omega_x=1.20$, $W=32.2$ MeV, $T_\perp=47.8$ MeV, $Y/Y_0=0.82$. For (b) V_{tr}: $\Delta z=3.53$ fm, $R=3.09$ fm, $\rho/\rho_0=1.94$, $\omega_\rho=2.71$, $\omega_x=1.20$, $W=32.2$ MeV, $T_\perp=44.6$ MeV, $Y/Y_0=0.89$.

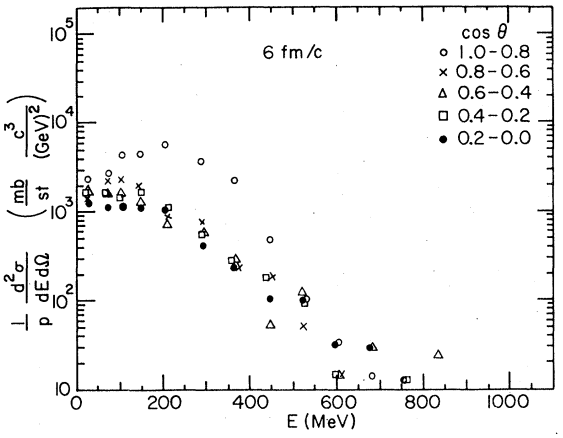

FIG. 11. As for Fig. 9. Results at $t=6$ fm/c. For V_{st}: $\Delta z=3.62$ fm, $R=2.68$ fm, $\rho/\rho_0=2.67$, $\omega_\rho=1.72$, $\omega_x=0.84$, $W=26.0$ MeV, $T_\perp=84.6$ MeV, $Y/Y_0=0.58$. [For V_{tr} (not shown): $\Delta z=3.53$ fm, $R=2.98$ fm, $\rho/\rho_0=1.94$, $\omega_\rho=1.85$, $\omega_x=0.85$, $W=33.6$ MeV, $T_\perp=80.0$ MeV, $Y/Y_0=0.60$.]

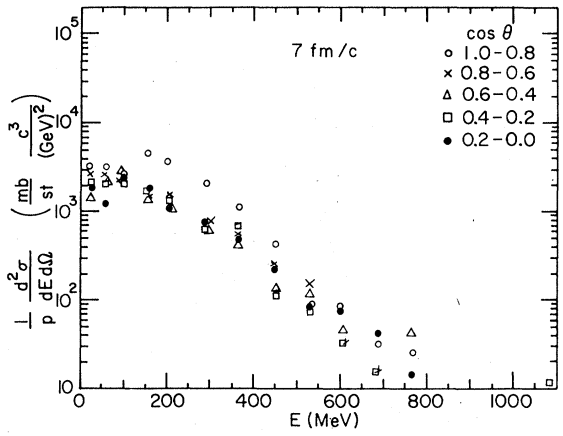

FIG. 12. As for Fig. 9. Results at $t=7$ fm/c. For V_{st}: $\Delta z=3.92$ fm, $R=2.90$ fm, $\rho/\rho_0=2.49$, $\omega_\rho=1.28$, $\omega_x=0.68$, $W=30.0$ MeV, $T_\perp=116.0$ MeV, $Y/Y_0=0.35$. [For V_{tr} (not shown): $\Delta z=3.85$ fm, $R=3.11$ fm, $\rho/\rho_0=1.93$, $\omega_\rho=1.22$, $\omega_x=0.68$, $W=31.5$ MeV, $T_\perp=117.6$ MeV, $Y/Y_0=0.30$.]

peak seems associated with the combination of large (not maximum) ρ and large relative momentum in the beam direction (nucleons approaching each other) thus giving a large interaction energy. The second peak seems associated with large radial momenta (nucleons receding from one another) and relatively large ρ. The dip occurs when the nucleons are close to each other and their average relative momentum is fairly small.

Figure 8 illustrates how the scattering equivalent potentials V_{st} and V_{tr} can give quite different results for W during the stage of large overlap. (Figure 7 illustrates the relatively smaller difference obtained for ρ.) The differences generally become larger with E_L, consistent with the momentum dependence of V_{tr} which occurs through V_p [Eq. (3)]. Also noteworthy is the large contribution to W due to V_p especially at higher energies, in view of the fact that V_p gives zero two-body scattering. (At 800 MeV, the contribution to W from V_p is about 50% of the total W for $t^* \lesssim 15$ fm/c.)

B. Momentum distributions

These, as a function of time, give a more detailed picture of the evolution of a collision than that just described.

Figures 9–16 are for $A_P = A_T = 20$, $E_L = 800$ MeV. One has $p_{\text{c.m.}} = 613$ MeV/c, and with $p_F \approx 250$ MeV/c: $p_+ \approx 863$ MeV/c ($E_+ \approx 400$ MeV) and $p_- \approx 363$ MeV/c ($E_- \approx 70$ MeV). The initial distribution, shown in Fig. 9, is consistent with these limits and at this energy lies entirely within the most forward cosθ bin ($0.8 \leq \cos\theta \leq 1$). Figures 17–24 are for $A_P = A_T = 20$, $E_L = 400$ MeV ($p_{\text{c.m.}} = 433$ MeV/c, $E_+ \approx 200$

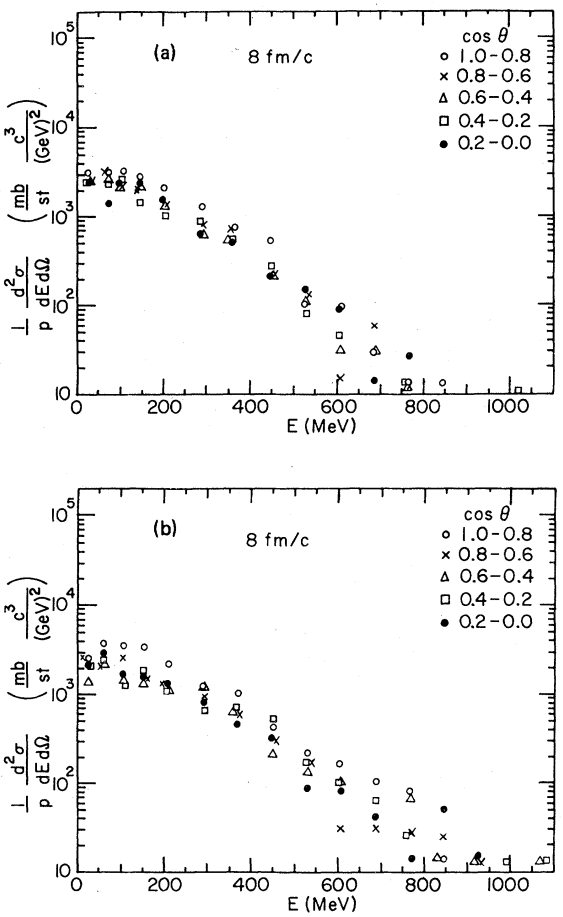

FIG. 13. As for Fig. 9. Results at $t = 8$ fm/c. For (a) V_{st}: $\Delta z = 4.10$ fm, $R = 3.40$ fm, $\rho/\rho_0 = 1.87$, $\omega_p = 1.13$, $\omega_x = 0.68$, $W = 30.1$ MeV, $T_\perp = 128.7$ MeV, $Y/Y_0 = 0.22$, $E_p \approx 75$ MeV, $\theta \approx 140$ MeV. For (b) V_{tr}: $\Delta z = 4.05$ fm, $R = 3.44$ fm, $\rho/\rho_0 = 1.67$, $\omega_p = 1.13$, $\omega_x = 0.66$, $W = 65.7$ MeV, $T_\perp = 143.3$ MeV, $Y/Y_0 = 0.14$.

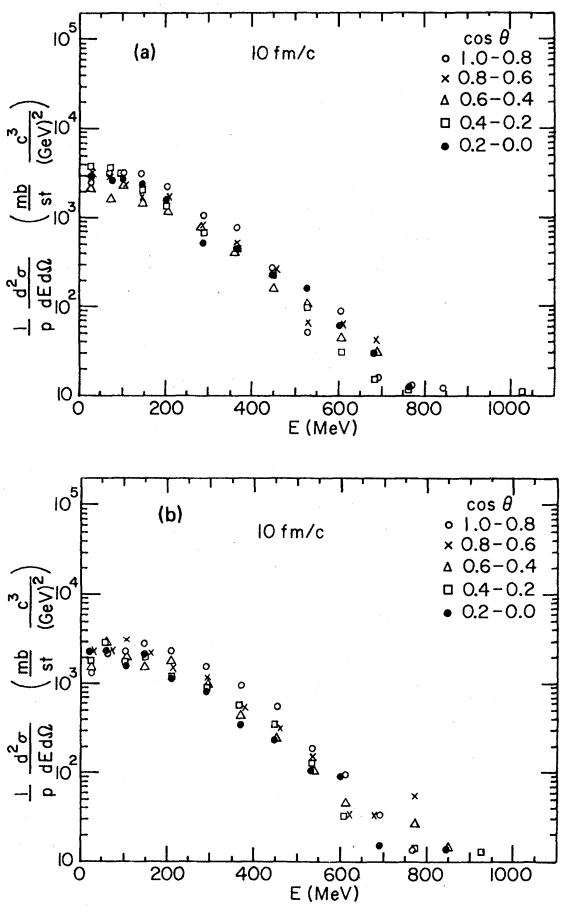

FIG. 14. As for Fig. 9. Results at $t = 10$ fm/c. For (a) V_{st}: $\Delta z = 4.34$ fm, $R = 4.75$ fm, $\rho/\rho_0 = 0.88$, $\omega_p = 1.09$, $\omega_x = 0.77$, $W = 15.9$ MeV, $T_\perp = 123.4$ MeV, $Y/Y_0 = 0.17$, $E_p \approx 55$ MeV, $\theta \approx 130$ MeV. For (b) V_{tr}: $\Delta z = 4.26$ fm, $R = 4.58$ fm, $\rho/\rho_0 = 0.88$, $\omega_p = 1.09$, $\omega_x = 0.77$, $W = 40.5$ MeV, $T_\perp = 132.8$ MeV, $Y/Y_0 = 0.11$, $E_p \approx 85$ MeV, $\theta \approx 150$ MeV.

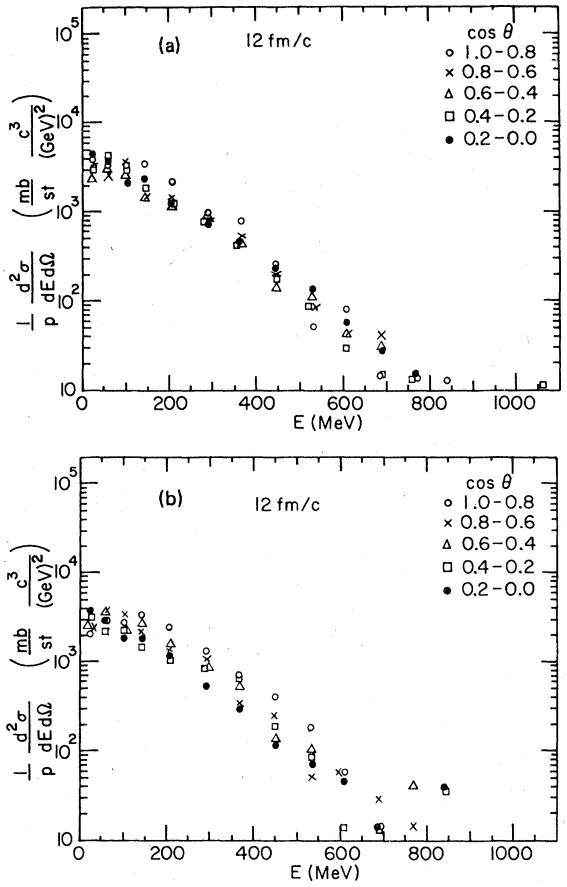

FIG. 15. As for Fig. 9. Results at $t=12$ fm/c. For (a) V_{st}: $\Delta z=4.56$ fm, $R=6.24$ fm, $\rho/\rho_0=0.42$, $\omega_p=1.09$, $\omega_x=0.85$, $W=7.6$ MeV, $T_\perp=118.9$ MeV, $Y/Y_0=0.16$, $E_p\approx 45$ MeV, $\theta\approx 130$ MeV. For (b) V_{tr}: $\Delta z=4.42$ fm, $R=6.00$ fm, $\rho/\rho_0=0.39$, $\omega_p=1.15$, $\omega_x=0.86$, $W=14.3$ MeV, $T_\perp=118.8$ MeV, $Y/Y_0=0.11$, $E_p\approx 70$ MeV, $\theta\approx 135$ MeV.

MeV, $E_-\approx 800$ MeV). The initial distribution is again consistent with these limits and also lies mostly, but not entirely, within the most forward cosθ bin. Figures 25–32 are for $A_P=A_T=40$, $E_L=400$ MeV. The initial distribution (Fig. 25) is almost the same as for $A_P=A_T=20$ since the internal energy is almost the same.

The initial "transparent" stage lasts until about maximum overlap; conditions are far from equilibrated or isotropic (e.g., the large values of ω_p and ω_x) and are at the opposite extreme from hydrodynamics. The momentum distribution is dominated by the progressively depleted "initial" distribution with its peak (for the forward direction) initially at the c.m. momentum $p_{\text{c.m.}}$ and its width determined by the Fermi momentum p_F.

The distribution during this stage is consistent with mostly single collisions between projectile and target nucleons, i.e., quasifree scattering.

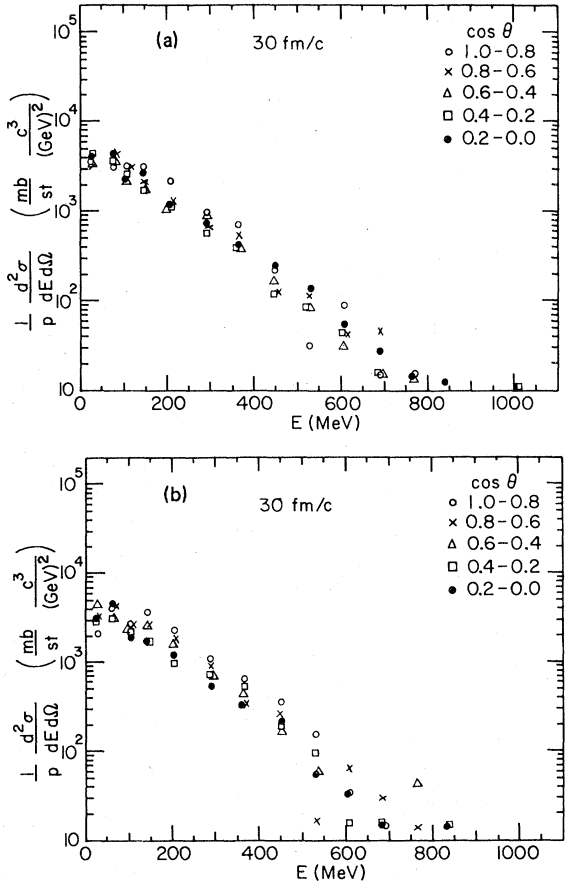

FIG. 16. As for Fig. 9. Results at $t=30$ fm/c. For (a) V_{st}: $\Delta z=6.38$ fm, $R=20.70$ fm, $\rho/\rho_0=0$, $\omega_p=1.08$, $\omega_x=1.01$, $W=1.4$ MeV, $T_\perp=115.7$ MeV, $Y/Y_0=0.15$, $E_p\approx 40$ MeV, $\theta\approx 124$ MeV. For (b) V_{tr}: $\Delta z=5.72$ fm, $R=20.40$ fm, $\rho/\rho_0=0$, $\omega_p=1.15$, $\omega_x=1.07$, $W=1.4$ MeV, $T_\perp=111.4$ MeV, $Y/Y_0=0.11$, $E_p\approx 50$ MeV, $\theta\approx 125$ MeV.

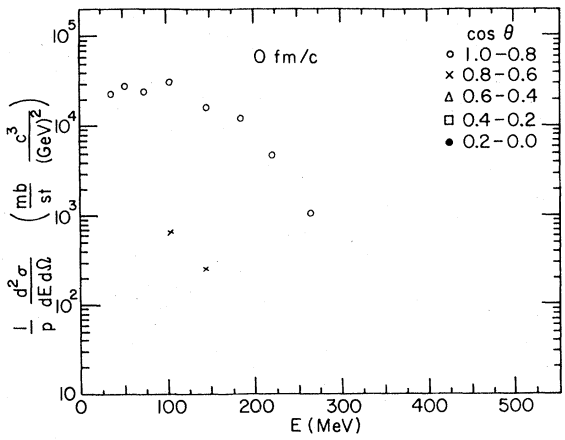

FIG. 17. Inclusive double differential cross section at $t=0$ fm/c for $A_P=A_T=20$, $E_L=400$ MeV and $b=0$. $\Delta z=0$ fm, $R=6.04$ fm, $\rho/\rho_0=0$, $\omega_p=3.98$, $\omega_x=3.61$, $W=28.1$ MeV, $T_\perp=13.6$ MeV, $Y/Y_0=1$. The energy bins are of size $\Delta E=20$ MeV for $E<100$ MeV and $\Delta E=40$ MeV for $E\geq 100$ MeV.

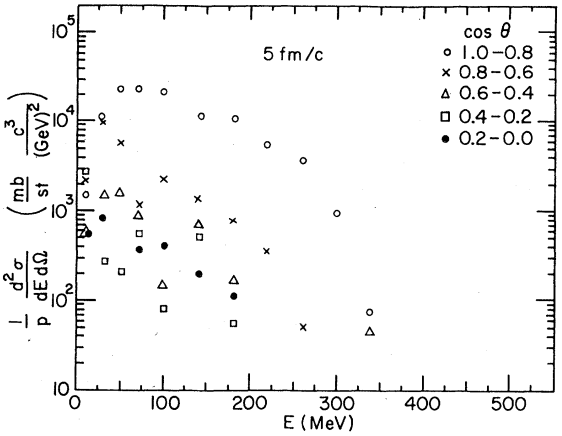

FIG. 18. As for Fig. 17 except at $t=5$ fm/c. For V_{st}: $\Delta z=2.31$ fm, $R=3.52$ fm, $\rho/\rho_0=1.38$, $\omega_p=3.27$, $\omega_x=1.88$, $W=37.5$ MeV, $T_\perp=20.4$ MeV, $Y/Y_0=0.97$. [For V_{tr} (not shown): $\Delta z=2.25$ fm, $R=3.67$ fm, $\rho/\rho_0=1.25$, $\omega_p=3.68$, $\omega_x=1.79$, $W=49.6$ MeV, $T_\perp=18.2$ MeV, $Y/Y_0=1.04$.]

Consistent with dominance of single scattering, the distribution of scattered nucleons has rather few high momentum components (i.e., ones with $p>p_F+p_F$). The high momentum components develop somewhat earlier (in terms of t^*) for lower E_L—consistent with a smaller mean-free path at lower energies.

During the earlier times (Fig. 18 for $t=t^*=5$ fm/c at 400 MeV) the angular distribution of the scattered nucleons (i.e., those for $\cos\theta<0.8$) is quite strongly forward peaked, whereas at later times (Figs. 10 and 11 at $t=5$ and 6 fm/c for 800 MeV and Fig. 19 at $t=7$ fm/c for 400 MeV) the dis-

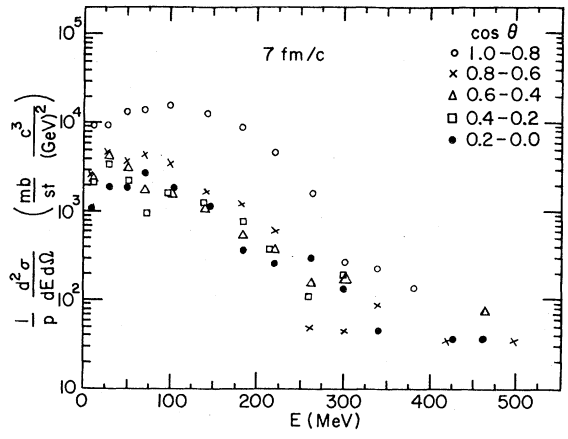

FIG. 19. As for Fig. 17 except at $t=7$ fm/c. For V_{st}: $\Delta z=3.12$ fm, $R=2.86$ fm, $\rho/\rho_0=2.20$, $\omega_p=2.03$, $\omega_x=1.23$, $W=38.4$ MeV, $T_\perp=33.0$ MeV, $Y/Y_0=0.83$. [For V_{tr} (not shown): $\Delta z=3.02$ fm, $R=3.16$ fm, $\rho/\rho_0=1.84$, $\omega_p=2.27$, $\omega_x=1.18$, $W=45.7$ MeV, $T_\perp=33.0$ MeV, $Y/Y_0=0.82$.]

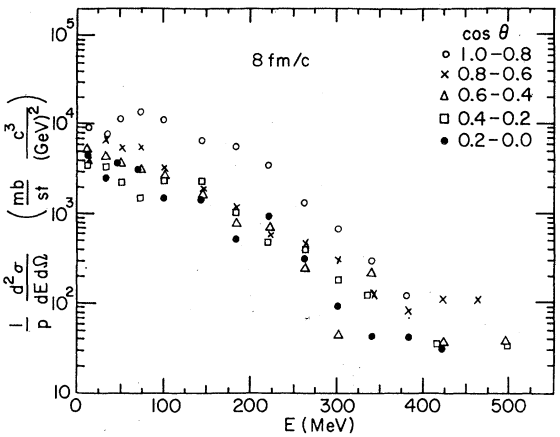

FIG. 20. As for Fig. 17 except at $t=8$ fm/c. For V_{st}: $\Delta z=3.42$ fm, $R=2.78$ fm, $\rho/\rho_0=2.35$, $\omega_p=1.61$, $\omega_x=0.96$, $W=38.0$ MeV, $T_\perp=50.3$ MeV, $Y/Y_0=0.59$. [For V_{tr} (not shown): $\Delta z=3.31$ fm, $R=3.09$ fm, $\rho/\rho_0=1.93$, $\omega_p=1.71$, $\omega_x=0.94$, $W=40.2$ MeV, $T_\perp=46.3$ MeV, $Y/Y_0=0.58$.]

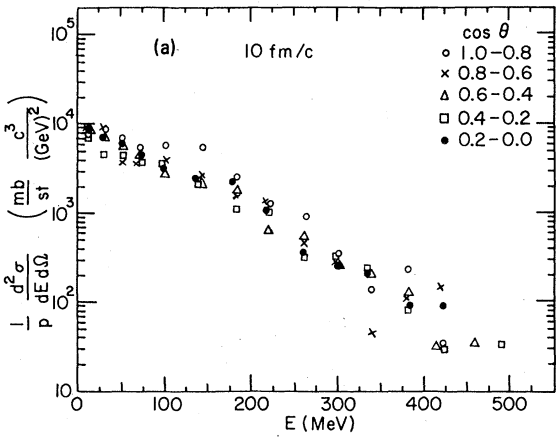

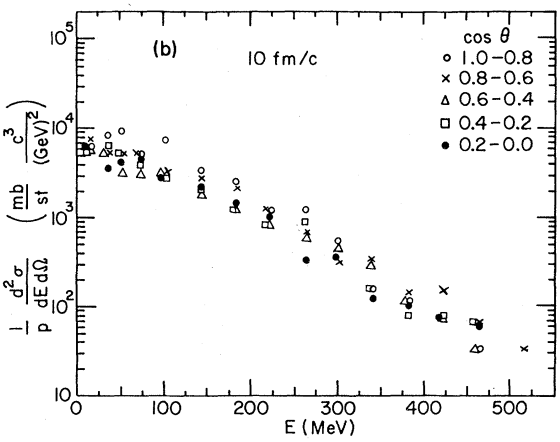

FIG. 21. As for Fig. 17 except at $t=10$ fm/c. For (a) V_{st}: $\Delta z=3.80$ fm, $R=3.19$ fm, $\rho/\rho_0=1.97$, $\omega_p=1.14$, $\omega_x=0.71$, $W=36.7$ MeV, $T_\perp=67.1$ MeV, $Y/Y_0=0.29$, $E_p\approx25$ MeV, $\theta\approx95$ MeV. For (b) V_{tr}: $\Delta z=3.68$ fm, $R=3.36$ fm, $\rho/\rho_0=1.52$, $\omega_p=1.15$, $\omega_x=0.71$, $W=46.6$ MeV, $T_\perp=69.2$ MeV, $Y/Y_0=0.15$, $\theta\approx90$ MeV.

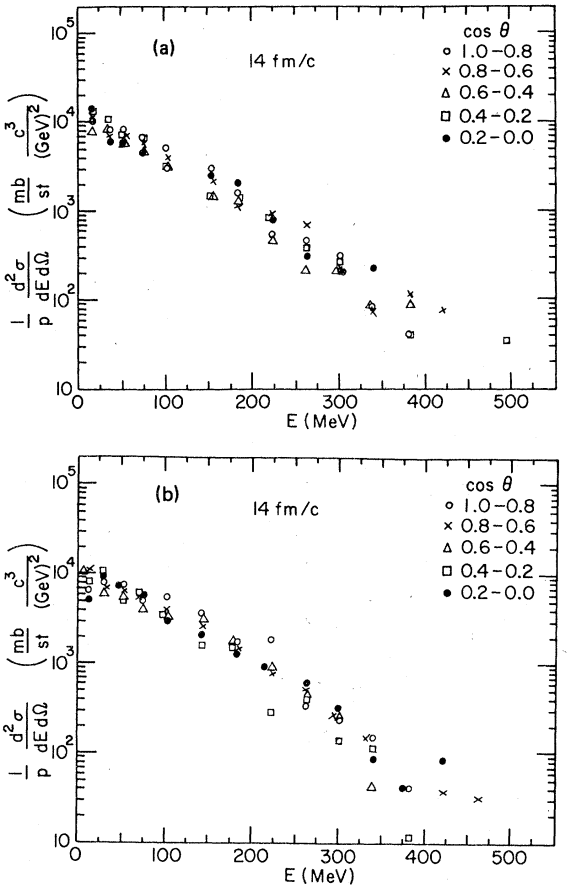

FIG. 22. As for Fig. 17 except at $t=14$ fm/c. For (a) V_{st}: $\Delta z=4.20$ fm, $R=5.00$ fm, $\rho/\rho_0=0.85$, $\omega_p=0.75$, $\omega_x=1.04$, $W=16.0$ MeV, $T_\perp=62.0$ MeV, $Y/Y_0=0.17$, $\theta\approx 75$ MeV. For (b) V_{tr}: $\Delta z=3.90$ fm, $R=4.90$ fm, $\rho/\rho_0=0.70$, $\omega_p=1.08$, $\omega_x=0.76$, $W=24.0$ MeV, $T_\perp=64.0$ MeV, $Y/Y_0=0.07$, $E_p\approx 20$ MeV, $\theta\approx 80$ MeV.

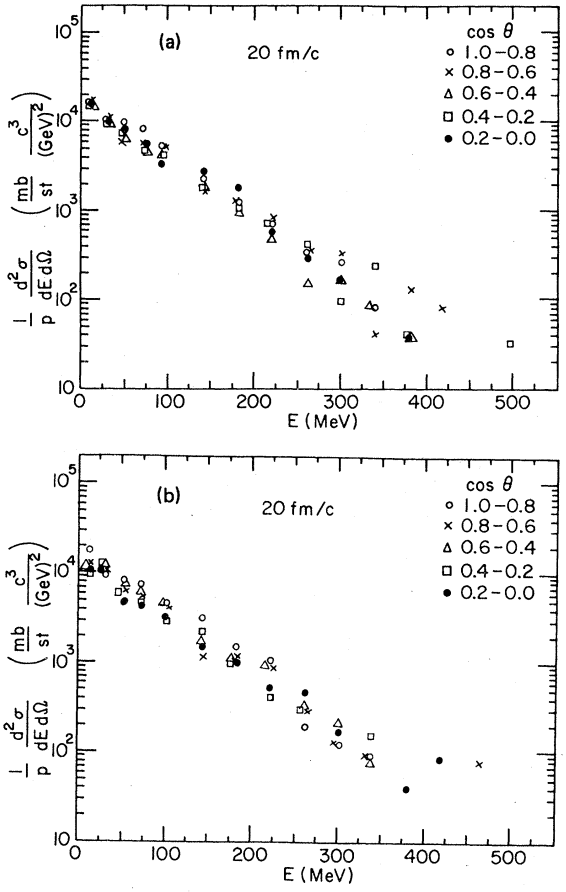

FIG. 23. As for Fig. 17 except at $t=20$ fm/c. For (a) V_{st}: $\Delta z=4.62$ fm, $R=8.20$ fm, $\rho/\rho_0=0.27$, $\omega_p=1.02$, $\omega_x=0.85$, $W=5.8$ MeV, $T_\perp=58.0$ MeV, $Y/Y_0=0.15$, $\theta\approx 70$ MeV. For (b) V_{tr}: $\Delta z=4.22$ fm, $R=8.05$ fm, $\rho/\rho_0=0.22$, $\omega_p=1.06$, $\omega_x=0.88$, $W=5.6$ MeV, $T_\perp=56.7$ MeV, $Y/Y_0=0.08$, $E_p\approx 15$ MeV, $\theta\approx 70$ MeV.

tribution is only moderately forward peaked. This seems consistent with our picture in which the effective two-body potential responsible for NN collisions for the early dilute conditions (dilute for scattering of projectile by target nucleons) is close to the complete two-body potential with its strongly forward peaked differential cross section, whereas for later, more dense conditions, the NN "collisions" will be due to an effective V_{short} which is closer to just the repulsive part of the potential and which has a more isotropic differential cross section. Moreover, multiple scattering may also be contributing significantly to the greater isotropy during the later times of the initial stage.

The distribution of scattered nucleons (i.e., those with $\cos\theta < 0.8$) shows some peaking in energy—at later times less for lower E_L—with the peak at a considerably lower energy than that ($\frac{1}{4}E_L$) of the initial (forward) distribution. As the latter becomes more strongly depleted, towards the end of the initial stage, its peak moves downward in energy, presaging the eventual development of an approximately common peak at all angles as discussed below.

It should be noted that already at the end of the initial stage ($t^*\approx 7$ fm/c) there has been a substantial reduction in the initial (projectile or target) rapidity ($Y/Y_0\approx 0.7$–0.8) corresponding to the loss of a major fraction of the initial beam kinetic energy [$T_\parallel/T_\parallel(0)\approx 0.5$–$0.6$] and also a large fractional increase in $T_\perp$ (to ≈ 0.5 of its maximum value). These large changes during the initial stage are then presumably mostly the result of single NN collisions which give rise to large momentum transfers as reflected in the momentum distributions (scattering to large angles).

The distributions for the scattering equivalent potentials, V_{st} and V_{tr}, show appreciable differ-

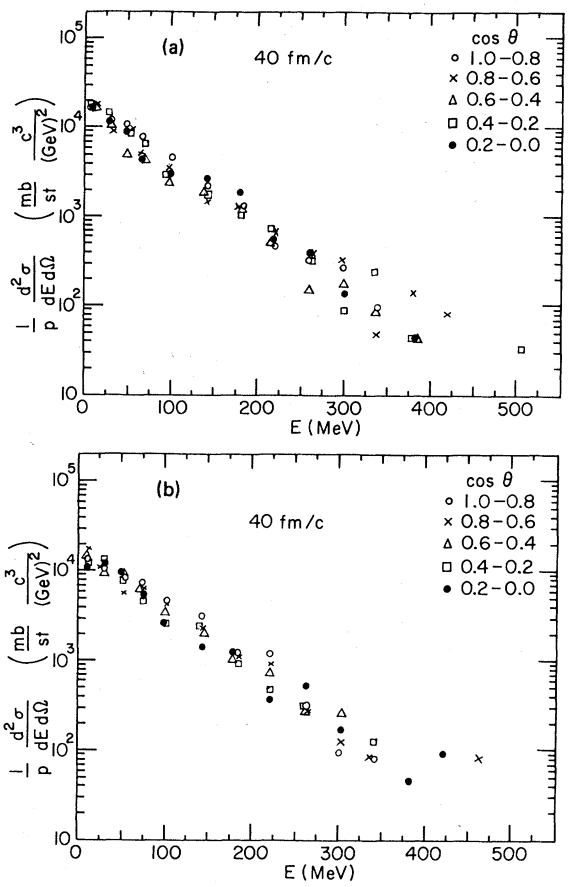

FIG. 24. As for Fig. 17 except at $t=40$ fm/c. For (a) V_{st}: $\Delta z=6.0$ fm, $R=19.40$ fm, $\rho/\rho_0=0.03$, $\omega_p=1.02$, $\omega_x=0.95$, $W=3.4$ MeV, $T_\perp=56.5$ MeV, $Y/Y_0=0.14$, $\theta\approx 65$ MeV. For (b) V_{tr}: $\Delta z=4.96$ fm, $R=19.21$ fm, $\rho/\rho_0=0.01$, $\omega_p=1.07$, $\omega_x=0.99$, $W=2.5$ MeV, $T_\perp=54.7$ MeV, $Y/Y_0=0.08$, $\theta\approx 65$ MeV.

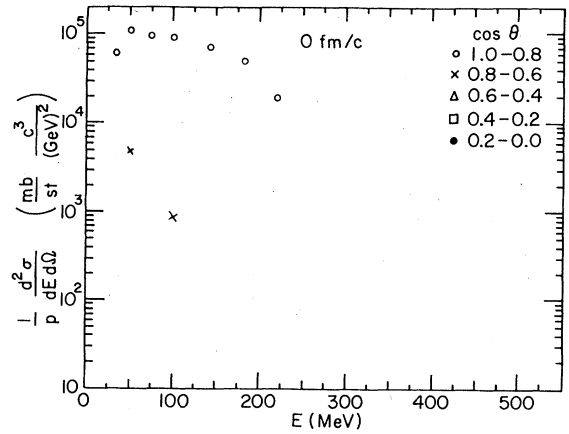

FIG. 25. Inclusive double differential cross sections at $t=0$ fm/c for $A_P=A_T=40$, $E_L=400$ MeV and V_{st} and $b=0$. $\Delta z=0$ fm, $R=6.36$ fm, $\rho/\rho_0=0.59$ (for $A_P=A_T=40$: $\rho_0=0.21$ fm^{-3}), $\omega_p=4.02$, $\omega_x=2.64$, $W=28.3$ MeV, $T_\perp=13.4$, $Y/Y_0=1$. The energy bins are the same as for $A_P=A_T=20$, $E_L=400$ MeV (see caption for Fig. 17).

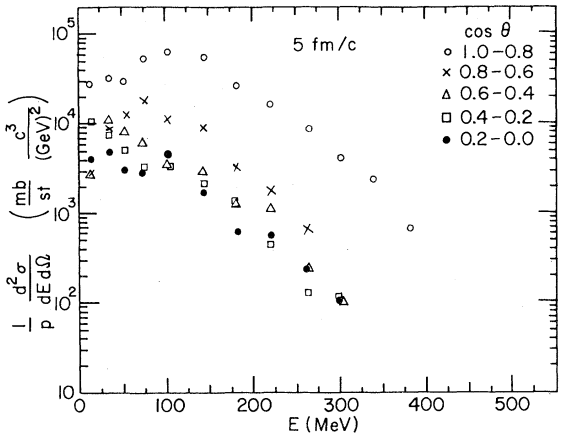

FIG. 26. As for Fig. 25 except at $t=5$ fm/c for V_{st}. $\Delta z=2.24$ fm, $R=4.02$ fm, $\rho/\rho_0=1.4$, $\omega_p=2.57$, $\omega_x=1.49$, $W=41.7$ MeV, $T_\perp=30.4$ MeV, $Y/Y_0=0.89$.

ences—especially for $E_L=800$ MeV—consistent with the larger effect of the momentum dependence of V_{tr} at higher energies. These differences are indicative of finite-range interaction effects. In particular, during the initial stage at 800 MeV, it is seen that (Figs. 10–13) the distribution for V_{tr} develops considerably more high momentum components than that for V_{st}. This seems to be related to the more negative potential energy/nucleon $-W$ for V_{tr} resulting from its momentum dependence. (Since the increase in W can only come from the overlapping projectile and target nucleons, with large relative momenta, this increase, via conservation of energy, can give quite large kinetic energies for just those nucleons.)

A "strong interaction" stage of relatively short duration follows. There is a rapid development

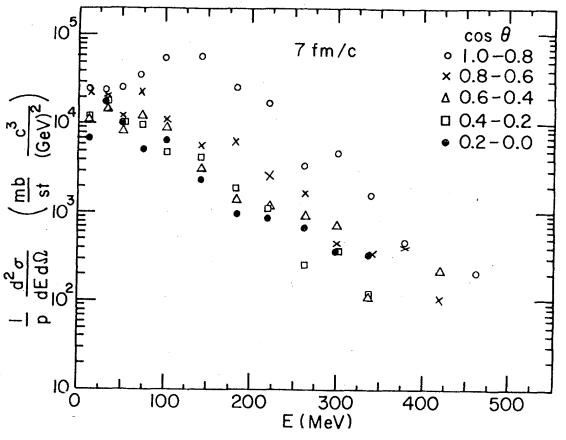

FIG. 27. As for Fig. 25 except at $t=7$ fm/c for V_{st}. $\Delta z=2.90$ fm, $R=3.60$ fm, $\rho/\rho_0=1.65$, $\omega_p=1.65$, $\omega_x=1.10$, $W=44.3$ MeV, $T_\perp=49.5$ MeV, $Y/Y_0=0.64$.

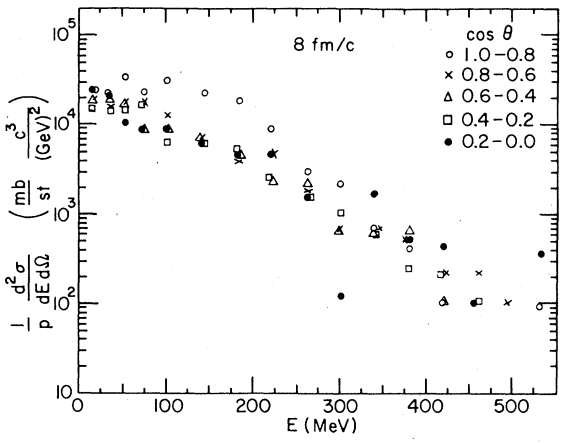

FIG. 28. As for Fig. 25 except at $t=8$ fm/c for V_{st}. $\Delta z=3.22$ fm, $R=3.51$ fm, $\rho/\rho_0=1.63$, $\omega_p=1.34$, $\omega_x=0.88$, $W=45.7$ MeV, $T_\perp=60.1$ MeV, $Y/Y_0=0.48$.

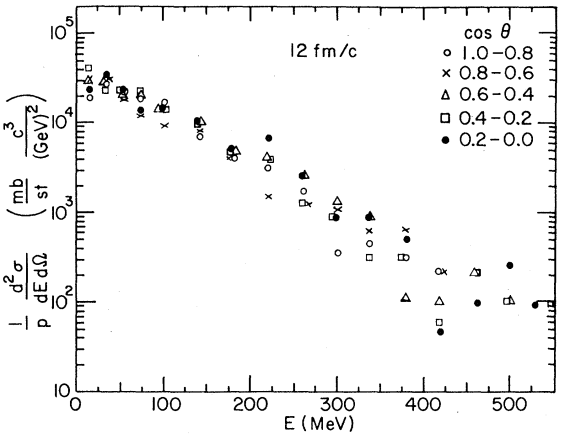

FIG. 30. As for Fig. 25 except at $t=12$ fm/c for V_{st}. $\Delta z=3.70$ fm, $R=4.75$ fm, $\rho/\rho_0=0.98$, $\omega_p=0.91$, $\omega_x=0.67$, $W=32.6$ MeV, $T_\perp=72.8$ MeV, $Y/Y_0=0.13$, $E_p\approx 25$ MeV, $\theta\approx 85$ MeV.

toward a much more isotropic and equilibrated momentum distribution, although the position distribution is still quite compressed in the beam direction even at the end of this stage (viz. the values of ω_p, ω_x). As already discussed, the densities are quite high, about $2\rho_0$ (somewhat larger for V_{st}) near the beginning of this stage and about ρ_0 near the end when the system is already expanding. Consequently there are frequent NN collisions and in particular much multiple scattering (this scattering and NN collisions during this stage generally being considered as due to V_{short}). The distribution of large momentum components, up to about 1.5 $(p_{c.m.}+p_F)$ (i.e. $\approx 2E_+$), becomes appreciable, strongly indicative of multiple scattering. For $E_L=800$ MeV the distribution for very large momenta (corresponding to $E\geq 600$ MeV) which develops at the end of this stage changes rather little during the subsequent expansion.

A "peak" (this is understood to include a bending over for small energies) which is roughly at the same energy for all angles has developed at the end of this or at the beginning of the subsequent expansion stage. This peak is quite pronounced at 800 MeV, but less so at lower E_L where it is sometimes little more than a flattening out near $E=0$ (especially for V_{st}), and which mostly disappears—presumably because of dissipation—during the expansion. The position of the peak is intermediate to that of the peak of the initial (forward) distribution (at $\frac{1}{4}E_L$) and that of the quasielastically scattered nucleons of the initial stage, and is presumably the result largely of further scattering of

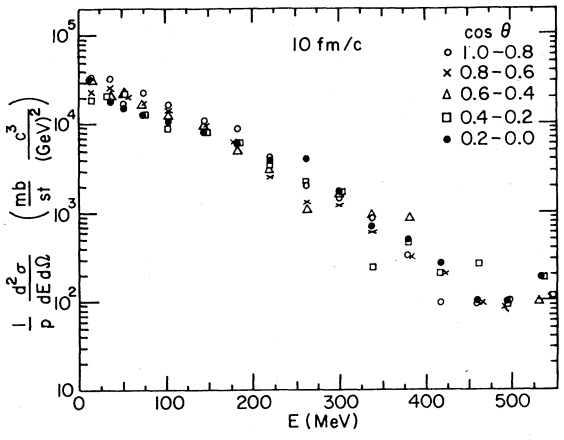

FIG. 29. As for Fig. 25 except at $t=10$ fm/c for V_{st}. $\Delta z=3.54$ fm, $R=3.94$ fm, $\rho/\rho_0=1.31$, $\omega_p=1.02$, $\omega_x=0.70$, $W=42.2$ MeV, $T_\perp=71.6$ MeV, $Y/Y_0=0.26$, $E_p\approx 25$ MeV, $\theta\approx 95$ MeV.

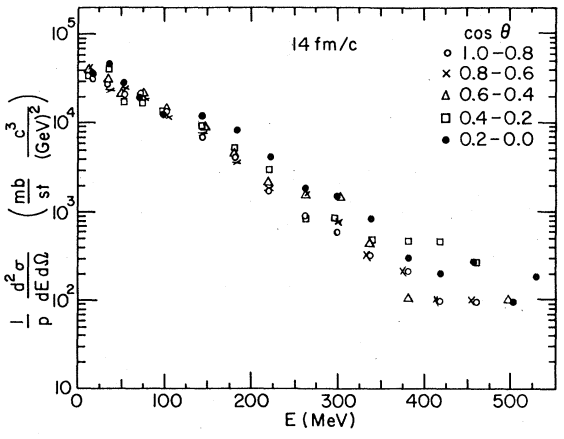

FIG. 31. As for Fig. 25 except at $t=14$ fm/c for V_{st}. $\Delta z=3.78$ fm, $R=5.70$ fm, $\rho/\rho_0=0.70$, $\omega_p=0.88$, $\omega_x=0.68$, $W=23.0$ MeV, $T_\perp=70.0$ MeV, $Y/Y_0=0.08$, $E_p\lesssim 20$ MeV, $\theta\approx 80$ MeV.

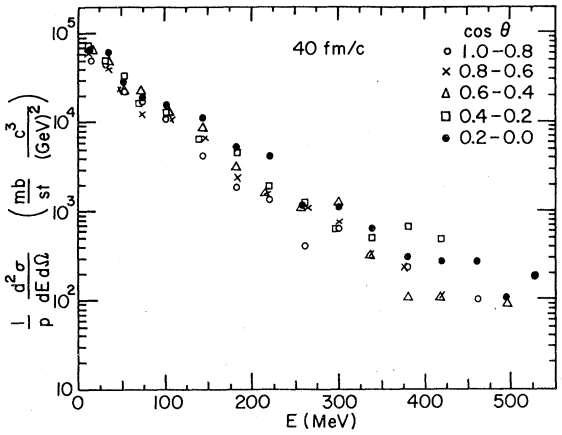

FIG. 32. As for Fig. 25 except at $t=40$ fm/c for V_{st}. $\Delta z=4.62$ fm, $R=19.90$ fm, $\rho/\rho_0=0$, $\omega_\rho=0.84$, $\omega_x=0.78$, $W=4.3$ MeV, $T_\perp=60.7$ MeV, $Y/Y_0=0.06$, $\theta\approx 70$ MeV.

these scattered nucleons with the nucleons in the depleted "initial" distribution, this scattering due to V_{short} taking place in the average potential $\overline{V}$ due to V_{long}. The development of an approximately common peak seems a completion of the development already occurring towards the end of the initial stage when the peak of the depleted "initial" distribution started moving down in energy.

There are appreciable differences between the distributions for V_{st} and V_{tr}, related to differences in potential energy and also to more rapid thermalization, i.e., greater dissipation for V_{st} than for V_{tr} as discussed further below.

The final expansion stage is (somewhat arbitrarily) considered to begin when the densities are about ρ_0, and when $T_\perp$ is near its maximum value. The single peak which has developed either shortly before or (for V_{tr} at 800 MeV) shortly after the beginning of the expansion stage, moves down in energy roughly in step with the increase of potential energy. Concurrently there is some increase in the steepness of the distribution above the peak, i.e., a decrease in θ if fitted with a Maxwell-Boltzmann distribution $e^{-E/\theta}$. This decrease is also consistent with the increase in potential energy. At 800 MeV there is, however, little change in the very high momentum components (i.e., those with $E\gtrsim 600$ MeV).

Although the very presence of the peak indicates incomplete thermalization, its movement in step with the potential energy (and also the associated increase in steepness above the peak) indicates that the momentum distribution adjusts itself to the changing average potential $\overline{V}$ during the expansion; this adjustment—consistent with energy conservation—is then brought about by the work done by the forces corresponding to $\overline{V}$. The approximate agreement of the shift in peak position with the change in potential energy is then accounted for if W is mostly due to $\overline{V}$, i.e., due to V_{long}. This is expected during the expansion stage since then $\rho<\rho_0$ and the contribution of the repulsive core (i.e., of V_{short}) to W is quite small for such conditions. Collisions (due to V_{short}) are expected to lead mainly to dissipation during the expansion and to manifest themselves in increasing thermalization. At 800 MeV the very fast nucleons presumably escape near the beginning of the expansion stage from the dense interaction region where $\overline{V}$ is large, and thus do not have the opportunity to adjust to $\overline{V}$ or to show as pronounced collective effects as do the slower nucleons.

Perhaps the most significant result is that there are quite pronounced differences in the peak positions for V_{st} and V_{tr} during the earlier expansion phase, which are indicative of finite-range, in particular potential-energy effects, but that finally these differences almost completely disappear. The differences in peak position are consistent with the differences in the potential energy for the two potentials, in agreement with the above picture. The differences are quite large especially during the expansion stage for 800 MeV. However, for 800 MeV, where the peaks persist rather distinctly to the final asymptotic distributions, there are finally at most only slight and not very significant differences in the positions of the peaks for V_{st} and V_{tr}. This indicates that there is little sensitivity of the final (observable) distributions to potential energy effects, even when these final distributions are not fully thermalized. This is in spite of the significant differences at earlier times during the collision. This result—that there is *finally* very little difference in the distributions—is consistent with the above explanation of potential-energy dependent effects as primarily due to the average potential $\overline{V}$ due to V_{long}: thus late in the expansion the nucleons are mostly well separated (with little clustering) and correspondingly W and hence also $\overline{V}$ are small for both V_{st} and V_{tr}. There is no indication of any outward movement, to larger energies, of the peak, as might be expected from an increase of the radial (collective) velocity at the expense of internal energy during the expansion.[22]

The distributions become more thermalized during the expansion, with the peak becoming less pronounced; in fact this "peak" mostly disappears during the expansion except at 800 MeV and except for some final slight bending near $E=0$ for V_{tr} at 400 MeV. For distributions which are highly thermalized the temperature θ decreases during the expansion. This decrease corresponds to a decrease of kinetic energy, related to the increase of potential energy ($-W$) by $\frac{3}{2}\Delta\theta=\Delta W$, as required

by the conservation of energy for a Maxwell-Boltzmann distribution: $\frac{3}{2}\theta = \frac{1}{4}E_L - B + W$, where B is the (initial) binding energy. [Thus, e.g., for the final distribution ($t = 40$ fm/c) for $A_P = A_T = 20$, $E_L = 400$ MeV (Fig. 24) one obtains $\theta \approx 65$ MeV which is consistent with energy conservation to the accuracy to which can be determined from the slope of the distribution ($\frac{3}{2}\theta \approx 97$ MeV, $\frac{1}{4}E_L - B + W = 95$ MeV since $W = 3$ MeV).] The more rapid thermalization at lower energies (it is most rapid at the lowest energy $E_L = 117$ MeV) is consistent with a shorter mean-free path at lower energies.

The increasing degree of thermalization during the expansion, due to the dissipative effects of the NN collisions (due to V_{short}), is presumably associated with a corresponding increase in entropy.[24] (The density distribution during the earlier and most significant stage of the expansion is quite anisotropic and hence one expects large velocity gradients and correspondingly large dissipation during this period.) This result, that the expansion seems not to be isentropic, demonstrates the importance of dissipative effects for HE-HI collisions—even for the expansion stage—and the need to include such effects, e.g., in hydrodynamic calculations.

At 800 MeV where the final distribution still has a peak, this peak is perhaps slightly less distinct for V_{st} than for V_{tr}, consistent with larger dissipative effects for V_{st}. Such a difference, if real, must then be attributed to finite-range interaction effects on dissipation, since the two potentials are scattering equivalent. In any case as already remarked, the differences in the final distributions are, at most, quite small even at 800 MeV. At lower energies at which there is almost complete thermalization the distributions are effectively identical, except possibly for slight differences for the very high momentum nucleons; however, these differences cannot be considered as particularly significant in view of the limited statistics involved.

A striking effect which, at 400 MeV, has developed for $A_P = A_T = 40$ but not yet for $A_P = A_T = 20$, is the development of transverse directional peaking during the early part of this expansion (between 10 and 14 fm/c; Figs. 29–31), i.e., of a distribution larger perpendicular to the beam than along it. (This is clearly evident in the rise of the cross section for $\cos\theta < 0.2$ above that for $\cos\theta > 0.8$, and also in the values of ω_p.) This development is clearly a collective effect, which has set in for $A = 80$ but not yet for $A = 40$, and which is reminiscent of some hydrodynamic results.[21] Also noteworthy for $A_P = A_T = 40$ is the development of some concavity at small E later during the expansion ($t \gtrsim 14$ fm/c). The downward movement of the

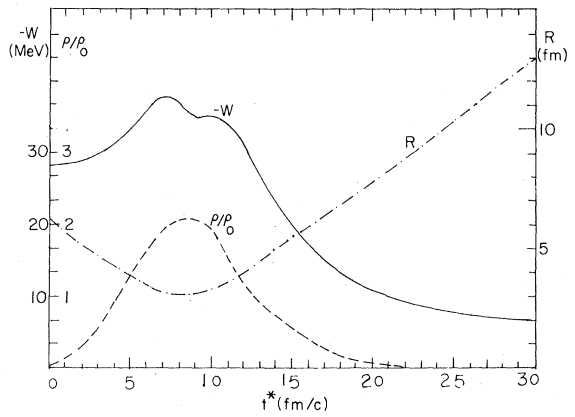

FIG. 33. Potential energy/nucleon $-W$, equivalent rms radius R, and ρ/ρ_0 vs reduced time t^* for $b = R$, $A_P = A_T = 20$, $E_L = 800$ MeV, and for V_{st}.

"peak," before ($t \lesssim 14$ fm/c) it is dissipated away, is consistent with the changes in W. It is noteworthy that this downward movement takes place at the same time that the transverse peaking is developing. We may interpret this simultaneous development as the result of collective (hydrodynamic) effects associated with approximate local equilibrium, brought about by collisions due to V_{short}, occurring in the presence of an average single-particle potential, due to V_{long}, which is associated with the downward movement of the peak during the expansion.

VIII. NONCENTRAL COLLISIONS AND IMPACT PARAMETER DEPENDENCE

Figures 33 and 34 are for $b = R$ (and $A_P = A_T = 20$, $E_L = 800$ MeV) and show the same quantities (as a function of t^*) as shown in Figs. 3 and 4 for $b = 0$. Nonequilibrium features are much larger than for

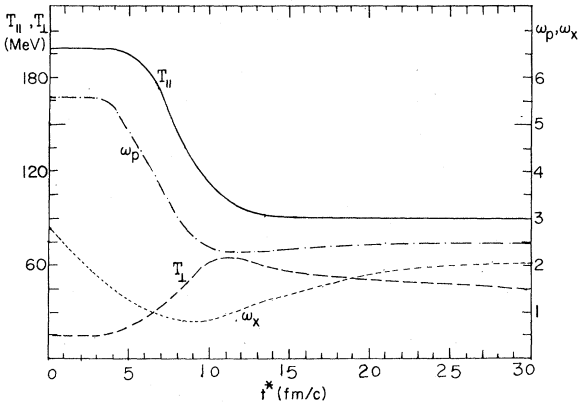

FIG. 34. Beam kinetic energy/nucleon in c.m. system $T_{\parallel}$, transverse kinetic energy/nucleon $T_{\perp}$, momentum asymmetry ω_p, and position asymmetry ω_x vs t^* for $b = R$, $A_P = A_T = 20$, $E_L = 800$ MeV, and for V_{st}.

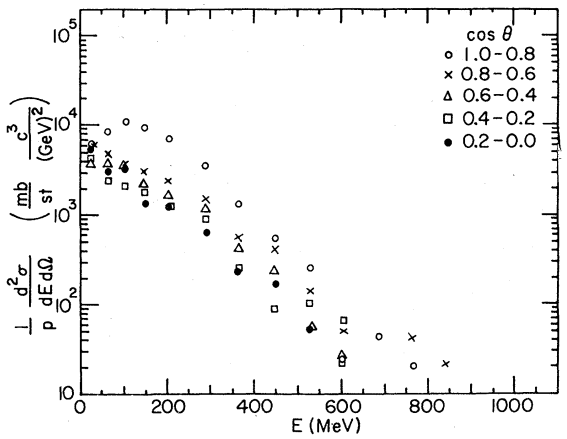

FIG. 35. Inclusive double differential cross sections at $t=30$ fm/c for a noncentral collision with $b=0.5R$ and for $A_P=A_T=20$, $E_L=800$ MeV. The energy bins are as for Fig. 9. For V_{st}: $\Delta z=9.80$ fm, $R=20.63$ fm, $\omega_p=1.52$, $\omega_x=1.42$, $W=2.1$ MeV. [For V_{tr} (not shown): $\Delta z=8.80$ fm, $R=20.45$ fm, $\omega_p=1.48$, $\omega_x=1.37$, $W=1.9$ MeV.]

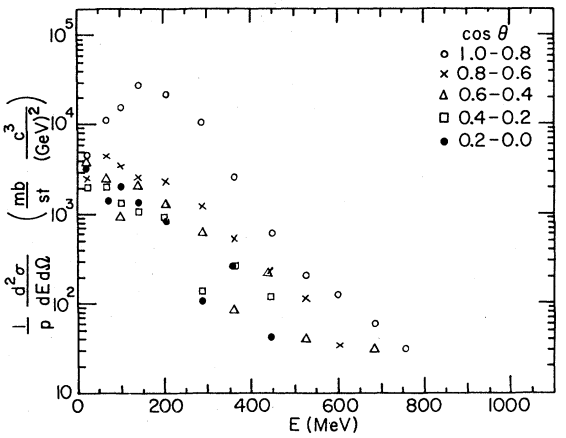

FIG. 37. Inclusive double differential cross sections at $t=30$ fm/c for a noncentral collision with $b=R$ and for $A_P=A_T=20$, $E_L=800$ MeV. The energy bins are as for Fig. 9. For V_{st}: $\Delta z=14.50$ fm, $R=20.00$ fm, $\omega_p=2.50$, $\omega_x=2.30$, $W=5.3$ MeV, $T_\perp=47.5$ MeV, $Y/Y_0=0.68$. [For V_{tr} (not shown): $\Delta z=13.70$ fm, $R=20.00$ fm, $\omega_p=2.35$, $\omega_x=2.18$, $W=4.7$ MeV, $T_\perp=51.8$ MeV, $Y/Y_0=0.62$.]

$b=0$; in particular, the final values show considerable memory of the initial state and a strong resemblance to fragmentation-type collisions.

The final momentum distributions only are shown for $b=0.5R$ (Figs. 35 and 36) and for $b=R$ (Figs. 37–39). The initial distributions are of course the same as for $b=0$. Only results for V_{st} are shown since the results for V_{tr} are not significantly different.

The final momentum distributions clearly show increasing nonequilibrium features as b increases; in particular, increasing memory of the initial distributions. For large b ($\gtrsim 1.5R$) they resemble fragmentation-type distributions with the final distributions quite close to the initial one, the differences being mainly due to evaporation and condensation. This trend with increasing b is consistent with the corresponding increase in the number of spectator nucleons and also with increasing transparency (Λ/L increases with b because L the nucleus-nucleus traversal length decreases). The final distributions for $b=0.5R$ clearly show large

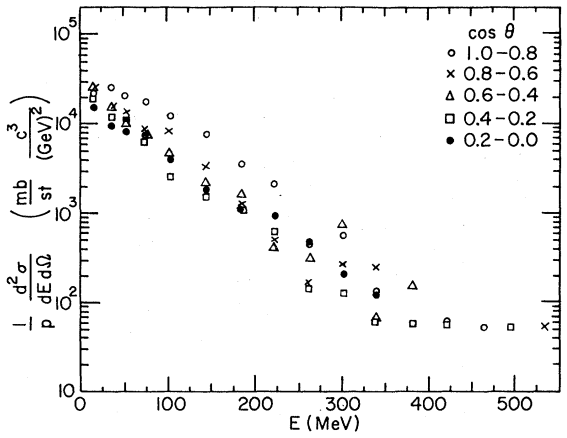

FIG. 36. Inclusive double differential cross sections at $t=30$ fm/c for a noncentral collision with $b=0.5R$ and for $A_P=A_T=20$, $E_L=400$ MeV. The energy bins are as for Fig. 17. For V_{st}: $\Delta z=6.83$ fm, $R=13.60$, $\omega_p=1.36$, $\omega_x=1.22$, $W=4.1$ MeV, $T_\perp=45.4$ MeV, $Y/Y_0=0.28$ [For V_{tr} (not shown): $\Delta z=6.44$ fm, $R=13.53$ fm, $\omega_p=1.37$, $\omega_x=1.23$, $W=3.4$ MeV, $T_\perp=45.3$ MeV, $Y/Y_0=0.26$.]

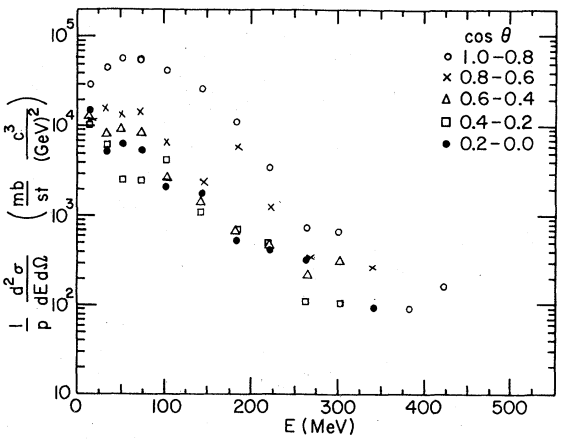

FIG. 38. Inclusive double differential cross sections at $t=30$ fm/c for a noncentral collision with $b=R$ and for $A_P=A_T=20$, $E_L=400$ MeV. The energy bins are as for Fig. 17. For V_{st}: $\Delta z=9.90$ fm, $R=13.40$ fm, $\omega_p=2.15$, $\omega_x=1.94$, $W=7.2$ MeV, $T_\perp=28.9$ MeV, $Y/Y_0=0.60$. [For V_{tr} (not shown): $\Delta z=9.36$ fm, $R=13.54$ fm, $\omega_p=2.06$, $\omega_x=1.84$, $W=6.6$ MeV, $T_\perp=29.6$ MeV, $Y/Y_0=0.54$.]

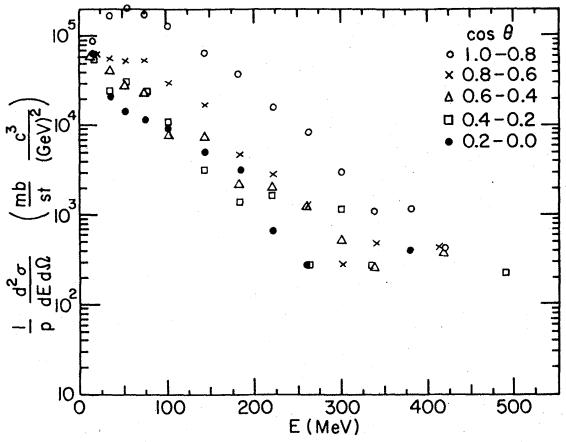

FIG. 39. Inclusive double differential cross sections at $t=30$ fm/c for a noncentral collision with $b=R$ and for $A_P=A_T=40$, $E_L=400$ MeV and for V_{st}. The energy bins are as for Fig. 17. $\Delta z=9.75$ fm, $R=14.10$ fm, $\omega_b=2.11$, $\omega_x=1.93$, $W=10.7$ MeV, $T_\perp=30.3$ MeV, $Y/Y_0=0.59$.

multiple scattering effects. Those for $b=R$ and $A_P=A_T=20$ show evidence of being much more dominated by single scattering (especially at 800 MeV); however, consistent with a larger traversal length, the final distribution for $A_P=A_T=40$ shows more evidence for multiple scattering than that for $A_P=A_T=20$. The momentum distributions for $b=0.5R$ and their evolution are discussed further below.

Some final rapidity distributions are shown in Fig. 40. These give a less detailed description than the momentum distributions but also illustrate the dependence on b. Thus for $b=0$ the final distribution is peaked at $Y\approx 0$, whereas for $b=R$ the distribution is doubly peaked with peaks at $Y/c\approx\pm 0.35$ compared with $Y_0/c=\pm 0.46$ at $t=0$ ($E_L=800$ MeV). The final impact-parameter averaged rapidity distribution is seen to resemble that for $b=R$. This double peaked feature, indicating strong memory of the initial state, is also consistent with a strong single scattering component both for the distribution for $b=R$ and for the impact parameter averaged distribution.

Figure 41 shows the final corrected values[25] of $T_\perp/\frac{1}{4}E_L$ and of the inelasticity I_f as functions of b for V_{st}. [The values for V_{tr} (not shown) are quite similar, especially for $T_\perp$; the values of I_f are slightly less for V_{tr} than for V_{st}.] Here $I=1-(Y/Y_0)^2$, where Y is the rapidity of the projectile (target) nucleons, and $I_f=I(t_f)$ is the final value. ($I=1$ and 0 correspond respectively to complete and no dissipation of the initial beam momentum.) I_f and $T_\perp/\frac{1}{4}E_L$ both decrease with b, becoming quite small for $b\gtrsim 1.5R$. For given b, I_f decreases as E_L decreases, consistent with a shorter mean-

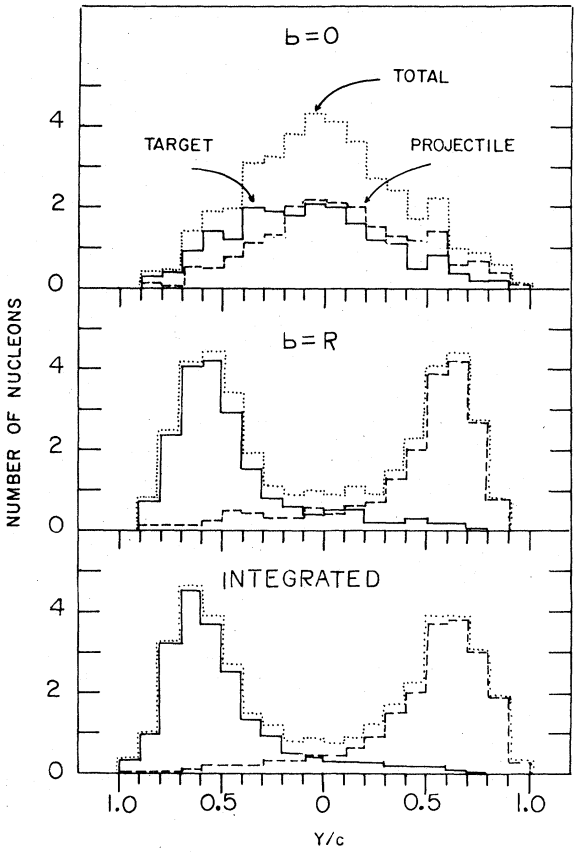

FIG. 40. Rapidity distributions for the projectile nucleons, target nucleons, and all nucleons vs Y/c for $t_f=30$ fm/c. The distributions are for $b=0$, $b=R$, and for the impact-parameter averaged distribution. The results are for $A_P=A_T=20$, $E_L=800$ MeV and V_{st}; nine impact parameters were used for the impact-parameter averaged cross section.

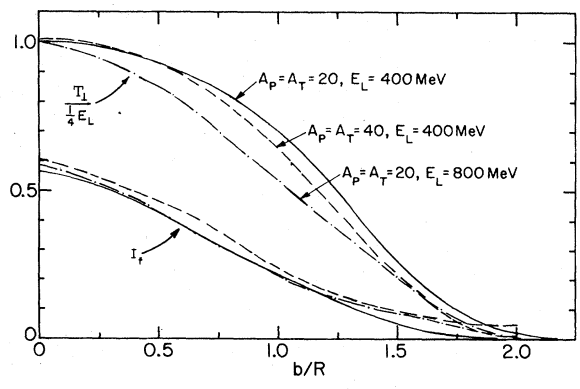

FIG. 41. The final inelasticity I_f (upper three curves) and the relative transverse kinetic energy $T_\perp/\frac{1}{4}E_L$ (lower three curves) vs b/R for the energies indicated. The results are for V_{st}.

free path Λ at lower energies. Also, I_f is smaller for larger A_P, A_T corresponding to larger dissipation appropriate to a larger traversal distance L. The *uncorrected* values of $T_\perp$ (given in the figure captions) for larger b (in particular for $b \gtrsim 1.5R$) are larger than expected. We attribute this mostly to the transverse energy associated with the initial internal momentum distribution. The figure in fact shows values of $T_\perp$ which have been corrected[25] to allow for this contribution which is relatively larger for larger b. For the corrected values we expect $T_\perp \approx 0$ for $b \gtrsim 2R$. This is seen to be so to a good approximation for $A_P = A_T = 20$. However, for $A_P = A_T = 40$, the corrected value is still about 5 MeV which must then be attributed to evaporation and condensation of the noninteracting nuclei.

Some results for the ratio W_f/W_0 of the final to the initial value of the potential energy/nucleon are shown in Table I. The values for V_{tr} are consistently slightly smaller than for V_{st}. This ratio is some measure of the number of nucleons which are bound or strongly clustered together at a late stage of the collision ($t^* \approx 40$ fm/c). For given E_L, W_f/W_0 increases with b and becomes quite appreciable for $b \gtrsim R$, presumably because of the increasing number of spectator nucleons which are less strongly affected than the participant nucleons and thus remain more strongly clustered together.

The large values of W_f/W_0 for $b = 0$ at $E_L = 117$ MeV are associated with partial "fusion." By this we mean a large quite persistent residue, approximately at rest in the c.m. system, with a large mass, $\gtrsim A/2$. Such fusion was already observed earlier[2] for $A_P = A_T = 50$, and also only at the lowest energy (117 MeV) considered and for $b \lesssim 0.25R$. The present evidence is quite similar although perhaps not quite as conclusive, in view of the smaller number of nucleons involved. The large residues are quite highly excited and will eventually evaporate; however, we did not follow the collision long enough to observe this. The large partial fusion indicates the possibility at relatively high energies ($E_L \approx 100$ MeV) of very large dissipation, in particular, thermal conduction. However, these results cannot be considered as too significant, in particular, because the CEOM approach is surely not applicable at such low energies, in particular because of blocking effects, especially for $p_{\text{c.m.}} < p_F$.

TABLE I. Final potential energies.

E_L(MeV)	b/R	$A_P = A_T$	$W_f/W_0 (W_0 \approx -28$ MeV) V_{st}	V_{tr}
800	0	20	0.05	0.05
400	0	20	0.12	0.09
400	0	40	0.15	
117	0	20	0.35	0.32
800	0.5	20	0.08	0.07
400	0.5	20	0.15	0.12
400	0.5	40		
800	1	20	0.19	0.17
400	1	20	0.26	0.23
400	1	40	0.38	

The *time development* (not shown) of the momentum distributions for $b = 0.5R$ (i.e., for moderately small b) shows features reminiscent of that for $b = 0$. Thus single NN collisions dominate during the early stage of the collision (e.g., for $t \lesssim 5$ fm/c for $E_L = 800$ MeV). Subsequently there is a strong interaction stage during which large momentum components develop. During the expansion stage the distribution of "scattered" nucleons (i.e., for $\cos\theta < 0.8$) shows evidence of increasing thermalization. There is again evidence for considerably more thermalization at lower E_L. Thus at 400 MeV the distribution for each individual angular bin, for $\cos\theta < 0.8$, approaches an exponential at late times. Also, there is considerably more depletion of the most forward (i.e., the "initial") distribution at 400 MeV. However, even at 400 MeV there are appreciable differences between the different angular bins for the scattered nucleons (i.e., those with $\cos\theta < 0.8$), the distribution of these nucleons thus being markedly forward peaked (in contrast to that for $b = 0$). This forward peaking is largest at 800 MeV, again consistent with less dissipation at this energy. There is some indication of a "peak" in energy for the scattered nucleons, this peak moving very roughly in step with the potential energy near the beginning of the expansion stage. However, this peak is much less clearly defined than for $b = 0$.

There are no appreciable differences in the final distributions for V_{st} and V_{tr}, although for earlier times (for $b = 0.5R$) there are again quite appreciable differences for the large momentum components, and also some indication that the peak for the scattered nucleons (e.g., at 10 fm/c for 800 MeV) occurs at a larger energy for V_{tr} than for V_{st}—again consistent with a more negative potential energy for the former. For $E_L = 400$ MeV the evolution is quite similar for V_{st} and V_{tr} with some slight indication of a peak (e.g., at ≈ 12 fm/c) at a slightly larger energy for V_{tr} than for V_{st}, again consistent with a correspondingly slightly more negative potential energy for V_{tr}. There is again also an indication of somewhat more rapid thermalization for V_{st}.

For $A_P = A_T = 40$ (at 400 MeV and for V_{st}) there are no qualitatively distinct features compared to $A_P = A_T = 20$; in particular, there is not the distinctive transverse peaking which was seen for $b = 0$.

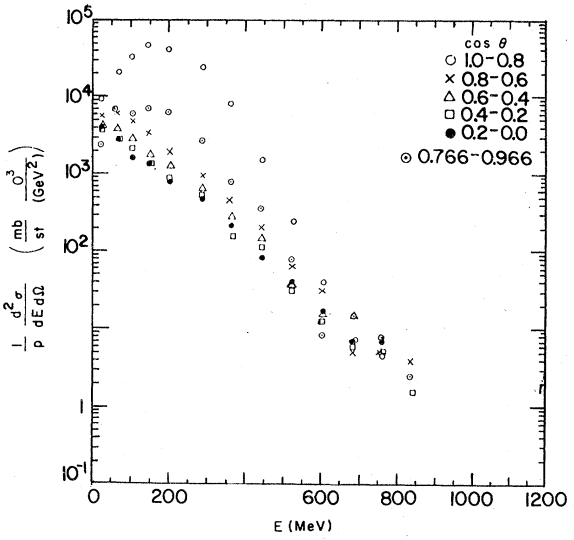

FIG. 42. Impact-parameter averaged inclusive double differential cross sections using nine impact parameters for V_{st}, $A_P = A_T = 20$, $E_L = 800$ MeV. The points ⊙ are for a midpoint value of 30°.

IX. IMPACT-PARAMETER AVERAGED INCLUSIVE CROSS SECTIONS

The impact-parameter averaged inclusive single-particle (proton) double differential cross sections are shown in Figs. 42–46. They have been obtained by an impact-parameter average of the cross sections (momentum distributions) for the individual impact parameters at the respective final times which depend on E_L and b.[26] For $A_P = A_T = 20$ at

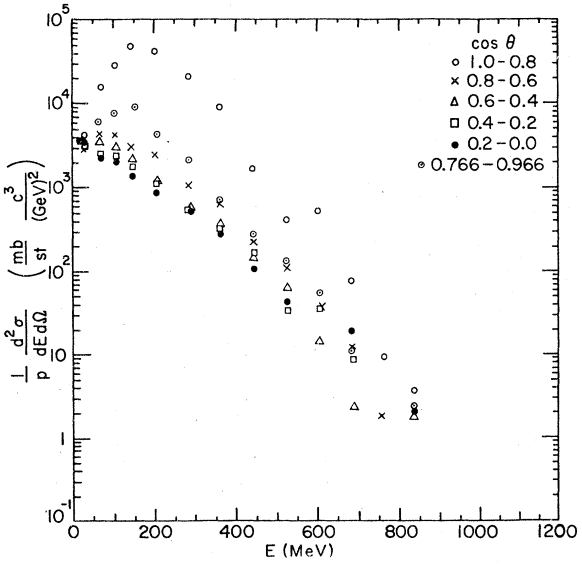

FIG. 43. As for Fig. 42 but for V_{tr}.

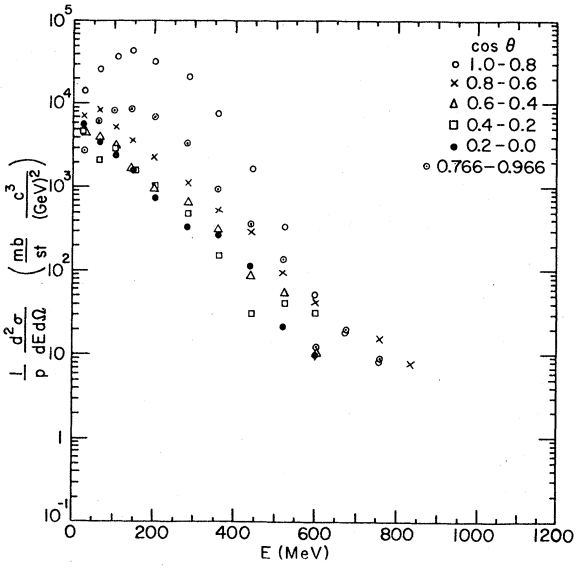

FIG. 44. As for Fig. 42 for V_{st} but using five impact parameters.

800 MeV, nine impact parameters ($n_b = 9$) were used for both V_{st} and V_{tr} ($0 \leq b \leq 2R$ with $\Delta b = 0.25R$). At 400 MeV we obtained results at only five impact parameters ($n_0 = 5$, $\Delta b = 0.5R$). (At 117 MeV only results for $b = 0$ and R were obtained and no meaningful average over impact parameter is possible.)

Figures 42 and 44 (for $A_P = A_T = 20$, $E_L = 800$ MeV and V_{st}) illustrate the difference between using $n_b = 9$ and 5. For $E \lesssim 600$ MeV the differences are fairly minor. However, for the high momentum

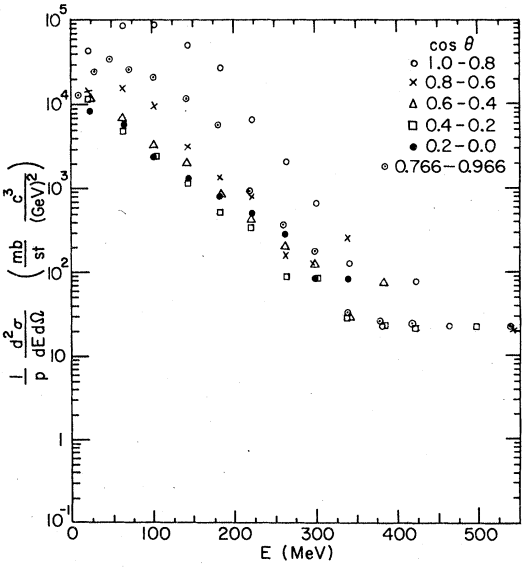

FIG. 45. Impact-parameter averaged inclusive double differential cross section for V_{st}, $A_P = A_T = 20$, $E_L = 400$ MeV using five impact parameters.

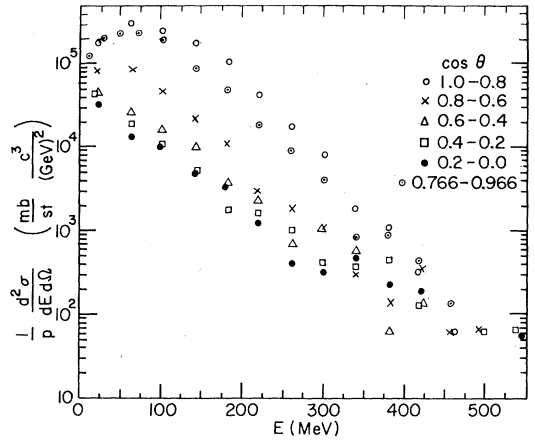

FIG. 46. Impact-parameter averaged inclusive double differential cross section for V_{st}, $A_P = A_T = 40$, $E_L = 400$ MeV using five impact parameters.

components there are appreciable differences. This is partly because of better statistics for $n_b = 9$,[27] but more importantly also because the results for $n_b = 5$ have relatively less contributions from smaller impact parameters (in particular, none from $b = 0.25R$) where there are relatively more high momentum components.

The results for $0.8 < \cos\theta < 1$ include all the small angle forward scattered nucleons and therefore strongly emphasize peripheral collisions (i.e., larger b). Thus this part of the cross section corresponds effectively to fragmentation collisions and strongly reflects the initial momentum distribution (with peak at $p_{\text{c.m.}}$ and with width determined by the initial internal momentum distribution). We also show results for $0.766 < \cos\theta < 0.966$ centered at $\cos\theta = 0.866$ corresponding to the experimental results for 800 MeV at this angle ($\theta = 30°$). Smaller values (<0.2) of the interval $\Delta\cos\theta$, with this same central value do not significantly change these results. Thus by excluding the contributions for $\cos\theta > 0.966$ ($\theta < 15°$) the dominant contribution of the very forward scattered nucleons is already excluded for the choice $\Delta\cos\theta = 0.2$.

Experimental results are shown in Fig. 47 for $A_P = A_T = 20$ (Ne + NaF) at 800 MeV. The values shown were interpolated from the published results[28] to correspond to our bins. The calculated values are in fair agreement except for $0.766 < \cos\theta < 0.966$. An important reason for the poorer disagreement in the forward direction is probably that our distributions do not have a sufficiently realistic surface.

A comparison of our results for $0 < \cos\theta < 0.2$ with the experimental 90° results is shown in Fig. 48. For 400 MeV the calculated results cut off at a relatively low energy, presumably because $n_b = 5$

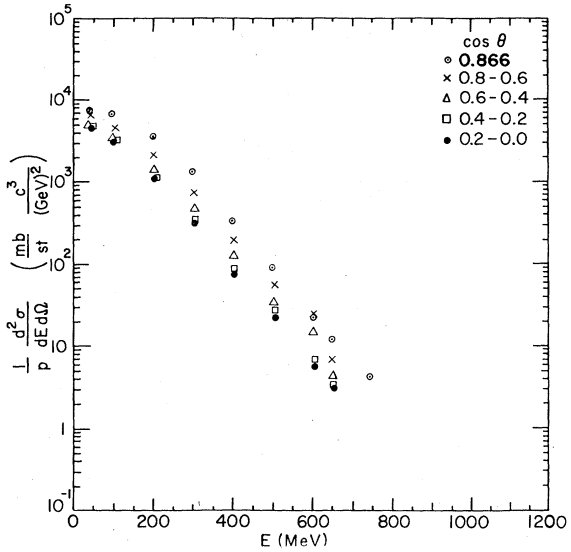

FIG. 47. Experimental invariant double differential cross sections for Ne+ NaF → p+ X at $E_L = 800$ MeV. The values shown were obtained by interpolation from the results of Ref. 28.

and the low impact-parameter results giving the high momentum components are under-represented. The temperatures for the calculated distributions (for $E \gtrsim 100$ MeV) for both V_{st} and V_{tr} are $\theta \approx 90$ MeV at 800 MeV and $\theta \approx 65$ MeV at 400 MeV with quite large errors ($\approx \pm 10$ MeV). Thus θ at 800 MeV is considerably less than the value ≈125 MeV for $b = 0$, but at 400 MeV is not significantly different (perhaps slightly less) than the temperature

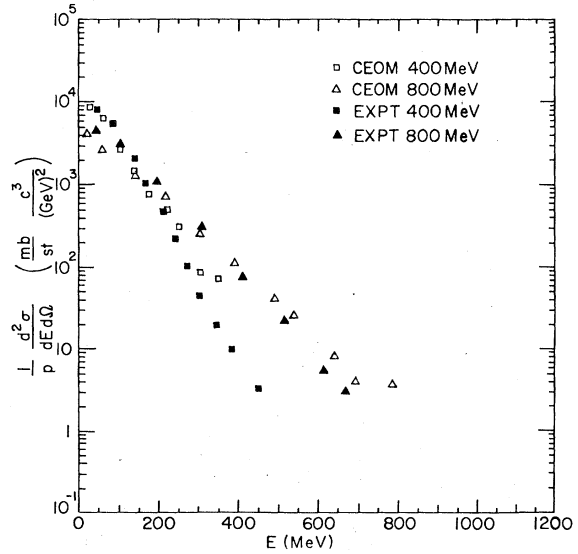

FIG. 48. The experimental values are the c.m. 90° values for Ne+ NaF (Ref. 28). The CEOM values are for $0 < \cos\theta < 0.2$, $A_P = A_T = 20$.

≈65 MeV for $b=0$. The larger difference at 800 MeV seems related to the larger transparency (smaller dissipation) at the higher energy. The corresponding 90° experimental values are 75 and 49 MeV at 800 and 400 MeV, respectively. Both these as well as the calculated values are consistent with the qualitative conclusion that there is relatively more complete thermalization at the lower energy. The figure indicates that the differences between the calculated and experimental values are probably not too significant in view of the rather large errors of the former.

Our results which are a composite of the distributions at different impact parameters clearly have a large single scattering component, especially for $A_P=A_T=20$ at 800 MeV, coming mostly from noncentral collisions. This seems at least qualitatively consistent with correlation measurements.[28] Consistent with greater dissipation at lower energies, there is less single scattering component at 400 MeV than at 800 MeV and for $A_P=A_T=40$ than for $A_P=A_T=20$.

The results for the scattering equivalent potentials V_{st} and V_{tr} are very similar and the slight differences can hardly be considered as significant in view of the errors. This result is of course consistent with that for the individual impact parameters. Thus also for the impact-parameter average results, finite-range interaction effects, in particular potential-energy effects, do not appear to be appreciable for the asymptotic cross sections, at least not for fairly light nuclei. We recall that during the collision there are appreciable differences in the results for V_{st} and V_{tr} for the individual impact parameters. Inadequacies and limitations of our calculated results are discussed in more detail in Sec. XI.

X. TESTS OF THERMAL MODELS

Some results of tests of thermal models (fireball and firestreak[7]) have previously been reported.[9] A partial test of thermal models was made for $b=0$ and $b=R$ by following three groups of projectile (target) nucleons initially in different impact-parameter ranges as shown in Fig. 49. For $b=0$ all three groups are "participant" nucleons, but for $b=R$ only the innermost group (I) are participants and groups II and III are spectators.

For $b=0$ (Fig. 50) there is fairly complete thermalization for groups I and II and somewhat less complete for group III consistent with larger transparency for the latter (L smaller, Λ/L larger). Thus for III there is, in particular, a non-negligible final rapidity. Results for the internal kinetic energy obtained for each groups of nucleons are consistent with these results. Thus for the final

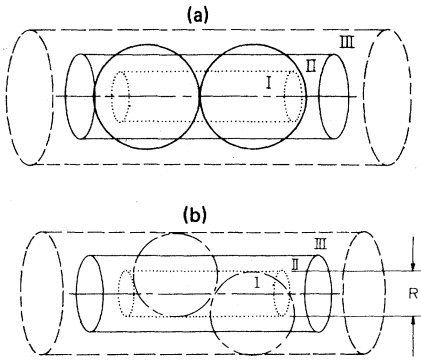

FIG. 49. Regions, I, II, III for $A_P=A_T=20$, for (a) $b=0$ and (b) $b=R$. For $b=0$ the regions are I ($r<1$ fm; $n=4.8$), II ($1<r<2$ fm; $n=9.7$), III ($r>2$ fm; $n=5.5$). For $b=R$ the regions are I ($r<1.3$ fm; $n=5.5$), II ($1.3<r<2.7$ fm; $n=9.5$), III ($r>2.7$ fm; $n=5.0$). n is the number of nucleons in the region: $\sum n=20$.

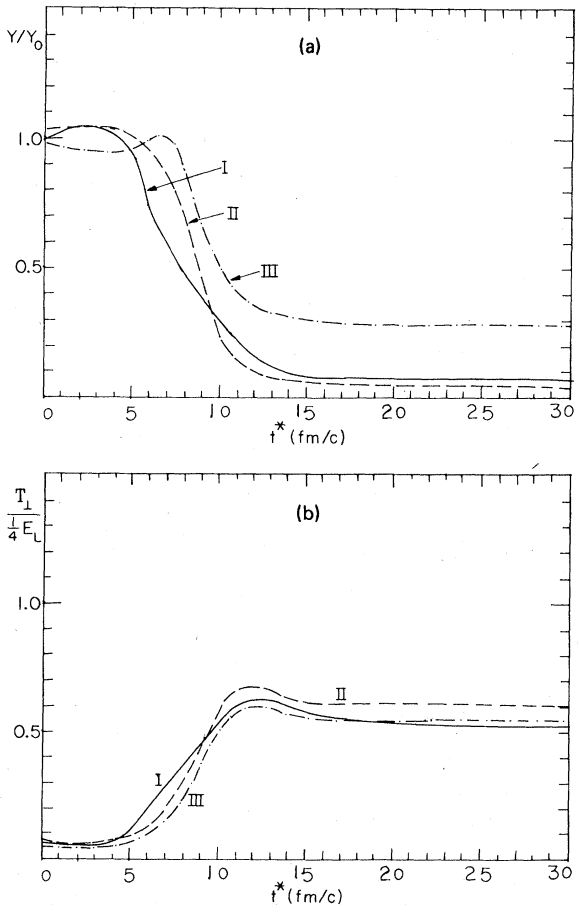

FIG. 50. (a) Y/Y_0 and (b) $T_\perp/\frac{1}{4}E_L$ vs t^* for a central collision $b=0$ and for $A_P=A_T=20$, $E_L=800$ MeV, and V_{st}, for nucleons initially in regions I–III shown in Fig. 49(a).

values at 800 MeV and for $A_P = A_T = 20$, one has $T_\perp^{(i)} = 105$ MeV, $T_\parallel^{(i)} = 52$ MeV, $e = 0.99(I)$; $T_\perp^{(i)} = 118$ MeV, $T_\parallel^{(i)} = 63$ MeV, $e = 1.07(II)$; $T_\perp^{(i)} = 109$ MeV, $T_\parallel^{(i)} = 77$ MeV, $e = 1.41(III)$. Here $e = 2T_\parallel^{(i)}/T_\perp^{(i)}$, where $T_\parallel^{(i)}, T_\perp^{(i)} \approx T_\perp$ are the internal kinetic energies, i.e., after the c.m. motion of the relevant group of nucleons has been subtracted out. Complete thermalization (but also the initial values) implies $e = 1$. At the lower energies, thermalization, in particular for group *III*, is even more complete than at 800 MeV—consistent with a shorter mean-free path at lower E_L. These results are in qualitative agreement with the thermal models which assume complete thermalization for each group. (The results for 800 MeV are of course consistent with the results for the momentum distributions which are finally not completely thermalized.)

For $b = R$ (Fig. 51) only the fireball model is tested. To test the firestreak model, each group, in particular the participant group *I*, would have to be further subdivided, and to obtain adequate statistics much larger ensembles would be needed. The appreciable final values of Y for group *I*, as well as the significantly smaller values of $T_\perp$ than for $b = 0$, at all energies, shows that the fireball model—not surprisingly—is inadequate for the participant nucleons.[29] The outermost spectator group *III* is only rather slightly affected by the collision, in agreement with the thermal models. However, the inner spectator group *II* is quite appreciably affected, suffering an appreciable increase in $T_\perp$, in qualitative disagreement with the thermal models. Thus an appreciable fraction of the transverse momentum of the participant nucleons is subsequently transmitted to the outer participant nucleons. Again, the results for the internal kinetic energies are consistent with these conclusions: thus for the final values at 800 MeV and for $A_P = A_T = 20$ one has $T_\perp^{(i)} = 75$ MeV, $T_\parallel^{(i)} = 84$ MeV, $e = 2.25(I)$; $T_\perp^{(i)} = 49$ MeV, $T_\parallel^{(i)} = 38$ MeV, $e = 1.54(II)$; $T_\perp^{(i)} = 29$ MeV, $T_\parallel^{(i)} = 16$ MeV, $e = 1.06(III)$. The peak values of $T_\perp$ are sucessively later for groups *I*, *II*, and *III*, again consistent with a progressive transmission of momentum from the participant nucleons, which first collide to the outer spectator nucleons.

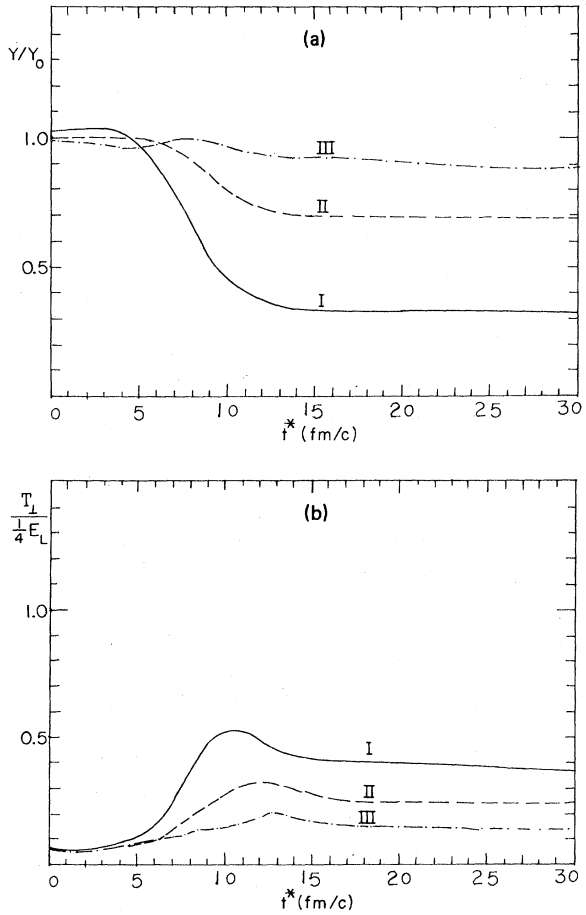

FIG. 51. As for Fig. 50 but for noncentral collision $b = R$ with I–III shown in Fig. 49(b).

XI. CONCLUSION

The present work is a continuation of previous work with the CEOM approach which is one of essentially three *a priori* approaches. Its unique features are that it is a completely microscopic, but classical, approach which can describe arbitrarily large nonequilibrium situations while simultaneously including finite-range interaction effects, in particular, potential-energy effects. An important aspect of CEOM calculations is then that of computer experiments which include certain elements of the physics of HE-HI collisions. Thus our use of the scattering equivalent potentials V_{st} and V_{tr} to explore the sensitivity to finite-range interaction effects, and tests of thermal models made by following selected groups of nucleons, are examples which emphasize this aspect.

We summarize some of our results and discuss limitations and possible improvements. For the evolution of central (or near central) collisions three stages may be distinguished:

1. An initial transparent stage during which single *NN* collisions mostly dominate. Conditions are far from isotropic or equilibrated and therefore far from hydrodynamic. At the end of this stage there is nevertheless a substantial reduction of the initial target (or projectile) rapidity Y and of the momentum asymmetry ω_p and a substantial increase in the transverse kinetic energy $T_\perp$.

2. A "strong interaction" stage of rather short duration follows. This is characterized by large

potential energies and densities (but never much more than twice the initial central density) and strong dissipation, as reflected in a rapid decrease in Y and ω_p and a rapid increase in $T_\perp$. There is evidence of much multiple scattering leading to an approximately isotropic momentum distribution with large momentum components but one which is not fully thermalized at the end of this stage. The density distribution then is, however, still quite strongly compressed in the beam direction and far from isotropic. Also toward the end of this stage or the beginning of the next a "peak" with its position at approximately the same momentum at all angles has developed. This peak appears to be an echo of the peak in the initial distribution due to the Fermi motion.

3. In the final expansion stage this "common" peak moves toward lower energies roughly in step with the decrease in magnitude of the potential energy/nucleon. This behavior of the peak is the first evidence for potential energy effects obtained in microscopic calculations. Concurrently there is mostly a corresponding increase in the steepness of the distribution above the peak (consistent with conservation of energy). The peak becomes progressively less pronounced during the expansion and, in fact, except for $A_P = A_T = 20$ at 800 MeV, the final distributions are mostly almost completely thermalized. The large degree of thermalization, and also the magnitude of the large momentum components, of the final distributions for $b = 0$ indicates that the single scattering component for zero impact-parameter collisions is small, and that these distributions, especially for the lower energies, are dominated by the effects of multiple scattering. Dissipation in fact seems quite large during the early expansion (for which there are then large density and velocity gradients) and which therefore is apparently not isentropic.

Quite generally dissipation is larger at lower energies and also for larger A_P, A_T, consistent with less transparency, i.e., larger Λ/L, appropriate to a larger cross section $\sigma^{(2)}$ at lower energies or a larger traversal distance L for larger A. During the collision there are very appreciable differences, in particular for $b = 0$, between the results for the scattering equivalent potentials (V_{st} and V_{tr}) for $A_P = A_T = 20$ for which such a comparison was made. Thus the densities, and especially the potential energies, are very different during the strong interaction and early expansion stages. Correspondingly, there are very appreciable differences in the momentum distributions; in particular the position of the common peak, once this has developed, correlates quite well with the corresponding average potential energy. Consistent with this correlation and with the small final potential energies, the final distributions—even for 800 MeV where these are not almost fully thermalized—are not significantly different, although there is some indication of more dissipation for V_{st} than for V_{tr}. Thus at least for light nuclei, large differences during interaction (also for $b > 0$) do not propagate to any significant extent into the asymptotic distributions. This is then true also for the impact-parameter averaged results.

For $A_P = A_T = 40$ (Ca+Ca) at 400 MeV transverse directional peaking of the momentum distribution develops for $b = 0$ during the early expansion stage, strongly suggestive of collective effects and reminiscent of the results of some hydrodynamic calculations. Again as for $A_P = A_T = 20$, the peak moves in step with the potential energy near the beginning of the expansion but then rapidly dissipates and disappears later during the expansion.

Noncentral collisions show increasing nonequilibrium features as the impact parameter increases, in particular, memory of the initial distribution—consistent with an increasing number of spectator nucleons as well as with increasing transparency Λ/L. For larger $b \gtrsim R$, the final distributions, especially for $A_P = A_T = 20$ at 800 MeV, are characterized by much single scattering. For $A_P = A_T = 40$ there is more multiple scattering. For smaller $b \lesssim 0.5R$ multiple scattering is large and much more pronounced than for $b = R$.

A partial test of thermal models indicates their qualitative validity for $b = 0$, consistent with the large degree of thermalization found for the momentum distributions. For $b = R$ only the fireball model is tested for the participant nucleons and—not unexpectedly—is adequate. The outer spectator nucleons are only slightly affected, consistent with thermal models; however, there is quite appreciable momentum transfer to the inner "spectator" nucleons.

The impact-parameter averaged results are in fair agreement with experiment, considering the inadequacies of the approach. Our results clearly have a very appreciable single scattering component arising mainly from the contributions with larger b. This seems at least qualitatively consistent with correlation measurements.

Our CEOM calculations have a number of deficiencies and limitations, as follows. Our initial configurations do not have a sufficiently realistic surface and also have somewhat too small a radius. This defect will then result in too much multiple scattering and thermalization. Also more adequate saturation properties for the two-body potentials are desirable. Our two-body potentials, which are fitted to $\sigma^{(2)}$, give too small values (≈ 0.5 of the empirical ones) for the longitudinal momentum-loss cross section $\sigma^{(1)}$.[8] This will result in too lit-

tle dissipation and too much emphasis on single scattering. Pauli blocking effects are not included; these will be especially important at the lower energies ($\lesssim$400 MeV) but might be significant even at 800 MeV. Neglect of blocking effects thus overestimates dissipation in our calculations, especially at lower energies. Thus a combination of the above, especially at the lower energies where relativistic effects and pion production are not too important, may well give too much dissipation, although to confirm this more refined calculations will be necessary. At 800 MeV neglect of relativistic effects and especially of pion production will be significant. Pion production might be expected to reduce the temperature of the nucleons. Production of light composites is large and will also affect the comparison between experiment and theory.[30]

Extensions and limitations. On the basis of our results we have suggested a kinetic equation (for the one-body distribution function) which includes finite-range interaction effects which are not included in the Boltzmann equation.

In this approach "collisions" are considered as due to the rapidly varying short-range, predominantly repulsive part V_{short} of the two-body potential, whereas the effect of the long range part V_{long} occurs through the corresponding average single-particle potential $\overline{V}$. Thus V_{short} enters the kinetic equation [Eq. (6)] through the collision term (of the Enskog form), and V_{long}–via $\overline{V}$ [Eq. (7)]–enters through a Vlasov-type term. Such an approach seems capable, for example, of explaining the simultaneous occurrence of potential and collective effects in the momentum distribution as seen in the results for $A_P = A_T = 40$.

This kinetic-equation approach probably can be rather naturally extended to include Pauli blocking effects through the inclusion of final state blocking factors in the collision term. (The one-body term, at least on its own, would preserve the phase space density and thus not give rise to a violation of the exclusion principle.) Such blocking effects cannot be included in a fully deterministic CEOM calculation, although some of the two-body effects of the exclusion principle may be included through use of a "Pauli" potential,[3] which may allow for some blocking effects in an average way. Blocking effects are more important at lower energies ($\lesssim$400 MeV) and our suggested kinetic-equation approach could perhaps be useful especially at lower energies ($50 \lesssim E_L \lesssim 200$ MeV?) where presently no adequate microscopic approach is available, i.e., one which would include collisions, including blocking effects, and finite-range interaction effects. Computational implementation of such a kinetic-equation approach seems capable of being achieved by suitable modification of the CEOM calculations by including appropriate probabilistic modifications.

At higher energies ($\gtrsim$600 MeV/nucleon but $\lesssim$1 GeV/nucleon appropriate to HE-HI collisions) pion production and relativistic effects will become important even if not dominant.

With use of potentials, i.e., with inclusion of finite-range interaction effects, a relativistic particle equation-of-motion description which involves a common time—i.e., a particle Hamiltonian or Lagrangian description—can be obtained to $O(v^2/c^2)$ by inclusion of retarded corrections to the nonrelativistic (static) potential.[31] Such a description is then Lorentz covariant (for both the trajectory and interactions) to $O(v^2/c^2)$. For a given nonrelativistic (static) potential V_{st}, the relativistic (retarded) corrections are not unique and some underlying (field theory) model is needed to obtain them. We have assumed that for $V_{\text{st}} = V_V + V_S$, of the form of Eq. (1), the short-range repulsive Yukawa potential V_V is due to a vector field and the long-range attractive potential V_S due to a scalar field. This then gives a unique relativistic potential to $O(v^2/c^2)$:

$$V_{\text{rel}} = V_{\text{st}} + V_{\text{ret}}\,, \tag{8}$$

$$V_{\text{ret}} = \frac{1}{4m^2c^2}\left[\left((\vec{p}_1\cdot\vec{p}_2)V_V(r) - \frac{(\vec{p}_1\cdot\vec{r})(\vec{p}_2\cdot\vec{r})}{r}\,\frac{dV_V}{dr}\right) + \left([-(\vec{p}_1-\vec{p}_2)^2 + \vec{p}_1\cdot\vec{p}_2]V_S(r) - \frac{(\vec{p}_1\cdot\vec{r})(\vec{p}_2\cdot\vec{r})}{r}\,\frac{dV_S}{dr}\right)\right]. \tag{9}$$

This depends on the same parameters (V_R, μ_R, V_A, μ_A) as V_{st}. These, however, are readjusted by refitting V_{rel} to $\sigma^{(2)}$ by two-body scattering calculations.[32] V_{rel} is Lorentz invariant to $O(v^2/c^2)$ for boosts. This is reflected by the fact that is depends on $\vec{p}_1, \vec{p}_2$ and not just through $\vec{p}_1 - \vec{p}_2$ as it would do if it were Galilean invariant.[33] Hamilton's equations must of course be used with inclusion also of the relativistic correction to the kinetic energy; thus to $O(v^2/c^2)$:

$$H = \sum_i \left(\frac{p_i^{\,2}}{2m} + \frac{p_i^{\,4}}{8m^3c^2}\right) + \sum_{i<j} V_{\text{rel}}(r_{ij}, p_i, p_j)\,. \tag{10}$$

So far we have made relativistic calculations only for single initial configurations, and comprehensive calculations for an ensemble remain to be made. An alternate suggestion to include relativistic effects, which ignores acceleration of the source particles, has been made by Wilets *et al.*[3]

Pion production can be included in CEOM calculations through coupling a classical pion field to the nucleons,[34] or on the lines used in cascade calcula-

tions. The latter would imply including also Δ's and π's in the CEOM calculations. Our suggested kinetic-equation approach would allow, fairly naturally, inclusion of pion production on the lines of cascade calculations (effectively through the collision term and through inclusion of Δ's and π's). Furthermore, classical field production, due to average changes in the nucleon source density, could possibly be included via Vlasov-type terms.

On a more restricted level, within the framework of nonrelativistic CEOM calculations, it is very desirable to have two-body potentials which have more adequate scattering properties, in particular, which fit both $\sigma^{(1)}$ and $\sigma^{(2)}$, and which can also give more adequate and flexible equations of state. A step in the latter direction has been made by use of Pauli potentials by Wilets *et al.*[3] We are presently studing the use of more general momentum dependent potentials which depend on both available momentum (p_r and l), and which show promise of being able to describe both aspects more adequately.

To obtain significant results for correlations, in particular two-nucleon correlated cross sections or cross sections for composites and also for studies involving selected groups of a small number of nucleons (as for the test of the firestreak model), it is necessary to increase the ensemble size by at least an order of magnitude in order to obtain the needed improvement in statistics. This effectively implies the need for substantial reductions in computing times either through the use of faster computers or improvements in the trajectory integrations. More than a factor of 2 is probably difficult to achieve for the latter but may of course be possible through use of sufficient ingenuity. Such reductions are also very desirable for nonrelativistic calculations with more complicated momentum dependent potentials, for relativistic calculations (which take about five times as long as nonrelativistic ones with a static potential), and for calculations for heavier nuclei.

ACKNOWLEDGMENTS

We are grateful especially to J. E. Monahan, J. Randrup, P. J. Siemens, and L. Wilets for discussions, helpful suggestions, and communications concerning this work. This work was performed under the auspices of the U. S. Dept. of Energy.

*Present address: Physics Dept., University of Ioannina, Ioannina, Greece.

[1]Recent reviews of high energy heavy-ion collisions are M. Gyulassi, Lawrence Berkeley Lab. Report No. LBL-6594 (unpublished); J. R. Nix, Prog. Part. Nucl. Phys. 2, 237 (1979); A. Goldhaber and H. Heckman, Annu. Rev. Nucl. Part. Sci. 28, 161 (1978); *Proceedings of the Topical Conference on Heavy Ion Collisions, Fall Creek Falls State Park, 1977,* edited by E. C. Halbert, *et al.* (ORNL Report No. Conf.-770602, 1977); *Proceedings of the Symposium on Relativistic Heavy Ion Research* edited by R. Bock and R. Stock (GSI, Darmstadt, 1978), Vols. I, II; The 4th High Energy Heavy Ion Summer Study, Berkeley, 1978 [Lawrence Berkeley Lab. Report No. LBL-7766, UC-340, Conf-780766 (unpublished)]. Also M. Gyulassi, Ref. 30.

[2]A. R. Bodmer and C. N. Panos, Phys. Rev. C 15, 1342 (1977); also Refs. 8, 9, and 13.

[3]L. Wilets, E. M. Henley, M. Kraft, and A. D. MacKellar, Nucl. Phys. A282, 361 (1977); L. Wilets, Y. Yariv, and R. Chestnut, *ibid.* A301, 359 (1978); D. J. E. Callaway, L. Wilets, and Y. Yariv, *ibid.* A327, 250 (1979).

[4]J. P. Bondorf, H. T. Feldmeier, S. Garpman, E. C. Halbert, and P. J. Siemens, Z. Phys. 279, 385 (1976); W. Jaisli, H. Kuhlmann, and C. C. Noack, *Proceedings of the Symposium on Relativistic Heavy Ion Research* (Ref. 1), p. 365; E. C. Halbert, Oak Ridge Natl. Lab. report (unpublished).

[5]Y. Kitazoe, M. Sano, and K. Y. Yamamoto, J. Phys. Soc. Jpn. Suppl. 44, 386 (1978), and private communication.

[6]Collapsed nuclei and density isomers: E. Feenberg, and H. Primakoff, Phys. Rev. 70, 980 (1946); A. R. Bodmer Phys. Rev. D 4, 1601 (1971); in *The Nuclear Many-Body Problem*, edited by F. Calogero and C. Ciofi degli Atti (Editrice Compositori, Bologna, 1973), p. 509. Abnormal nuclear matter: T. D. Lee, Rev. Mod. Phys. 47, 267 (1975); J. Boguta, Argonne Natl. Lab. report (unpublished). Pion Condensates: A. B. Midgal, Rev. Mod. Phys. 50, 107 (1978); W. Weise, *Symposium on Relativistic Heavy Ion Research* (Ref. 1), p. 221. Quark matter: J. C. Collins and M. J. Perry, Phys. Rev. Lett. 34, 1353 (1975); G. Baym and S. A. Chin, Phys. Lett. 62B, 241 (1976); G. F. Chapline and M. Nauenberg, Nature 264, 235 (1976); G. F. Chapline and A. K. Kerman, Lawrence Berkeley Report (unpublished); S. A. Chin and A. K. Kerman, Phys. Rev. Lett. 43, 1292 (1979).

[7]Fireball model: J. Gosset, H. H. Gutbrod, W. G. Meyer, A. M. Poskanzer, A. Sandoval, R. Stock, and G. D. Westfall, Phys. Rev. C 16, 629 (1977); Firestreak model: W. D. Myers, Nucl. Phys. A296, 177 (1978); J. Gossett, J. I. Kapusta, and G. D. Westfall, Phys. Rev. C 18, 844 (1978).

[8]A. R. Bodmer, *Proceedings of the Topical Conference on Heavy Ion Collisions* (Ref. 1), p. 309.

[9]A. R. Bodmer, *Proceedings of the Symposium on Relativistic Heavy Ion Research* (Ref. 1) p. 347.

[10]G. F. Chapline, M. H. Johnson, E. Teller, and M. S. Weiss, Phys. Rev. D 8, 4302 (1973); H. Stöcker, J. A. Maruhn, and W. Greiner, Phys. Rev. Lett. 44, 725 (1980) and references cited therefor earlier work of W. Greiner and collaborators; A. A. Amsden, F. H. Harlow, and J. R. Nix, Phys. Rev. C 15, 2059 (1977); A. A. Amsden, A. S. Goldhaber, F. H. Harlow, and J. R. Nix, *ibid.* 17, 2080 (1978); J. R. Nix in Ref. 1;

Y. Kitazoe, K. Matuoka, and M. Sano, Prog. Theor. Phys. 56, 860 (1976) and earlier papers cited.

[11]R. K. Smith and M. Danos, *Proceedings of the Topical Conference on Heavy Ion Collisions* (Ref. 1), p. 363; J. P. Stevenson, Phys. Rev. Lett. 41, 1702 (1978); Y. Yariv and Z. Fraenkel, Phys. Rev. C 20, 2227 (1979). The direct knockout model of S. E. Koonin, Phys. Rev. Lett. 39, 680 (1977), may be considered as a single-scattering approximation to cascade calculations or the Boltzmann equation.

[12]The calculations of Halbert *et al.* and of Noack *et al.* (Ref. 4) for hard spheres seem effectively equivalent to the use of the Enskog equation. A recent review of the latter is given by M. G. Velarde in *Lecture Notes in Physics* (Springer, Berlin, 1974), Vol. 31, p. 289.

[13]A. R. Bodmer, A. D. MacKellar, and C. N. Panos, Bull. Am. Phys. Soc. 22, 104 (1977); Proceedings of the Topical Conference on Heavy Ion Collisions (Ref. 1), p. 479.

[14]M. I. Sobel, P. J. Siemens, J. P. Bondorf, and H. A. Bethe, Nucl. Phys. A251, 502 (1975).

[15]For larger A a smaller number of configurations suffices to give approximately the same statistics (for single-particle inclusive cross sections) as for a smaller value of A. Roughly, one expects comparable statistics if the number of final nucleons is comparable. Thus for comparable statistics $N \propto 1/A$, and since the computing time for a single distribution is roughly proportional to A (because the interactions are of short range), the total computing time for ensembles giving about the same statistics is in fact about the same, independent of A (for $A_P = A_T$). Thus in effect the choice $N = 32$ and 21 for $A = 40$ and 80, respectively, gives somewhat better statistics for the latter.

[16]For $A_P = A_T = 20$, $E_L = 800$ MeV and for a central collision, the trajectory computing times for a single configuration are about 45 and 70 sec for V_{st} and V_{tr}, respectively, with use of an IBM 370/195 computer. For noncentral collisions, e.g., $b = R$, the times are somewhat less because the collision time is effectively shorter. The computing times for the analysis are considerably less than those for the trajectory computations.

[17]J. E. Monahan, C. M. Shakin, and R. M. Thaler, Argonne Natl. Lab. report (unpublished).

[18]For nucleon-nucleus scattering, cascade calculations including a single-particle potential are considered by K. Chen, Z. Fraenkel, G. Friedlander, J. R. Grover, J. M. Miller, and Y. Shimamoto, Phys. Rev. 166, 949 (1968).

[19]J. Knoll and J. Randrup, Nucl. Phys. A314, 427 (1979).

[20]See J. Hüfner, The 4th High Energy Heavy Ion Summer Study (Ref. 1), p. 135.

[21]See, in particular, the hydrodynamic calculations of Greiner and co-workers (Ref. 10).

[22]P. J. Siemens and J. O. Rasmussen, Phys. Rev. Lett. 42, 880 (1979).

[23]The bin sizes used for the energy are a compromise, achieved by trial and error, between statistics and energy resolution. We also tested for the effects of different parametrizations, namely bins corresponding to equal intervals of p^2 (i.e., of E, appropriate to $d^2\sigma/pdEd\Omega$) and of equal intervals of p^3 (appropriate to $d^2\sigma/dp^3d\Omega$). No appreciable differences were found between these two parametrizations.

[24]It is clearly of interest to obtain the change of entropy during the expansion.

[25]The correction was made using $T_\perp$ (corrected) $= T_\perp - cT_\perp(t=0)$, where $T_\perp(t=0) \approx \frac{2}{3}\overline{T}$ and $\overline{T} \approx 20$ MeV is the initial average internal kinetic energy and c is the ratio of the initial (nonoverlap) volume of the spectator nucleons to the initial total volume of all nucleons.

[26]Thus at 800 MeV, $t_f = 40$ fm/c for $b < R$, $t_f = 30$ fm/c for $R \leq b \leq 1.5R$, and $t_f = 20$ fm/c for $b > 1.5R$. Also, the average over impact parameter is quite insensitive to the details of how it is obtained, e.g., whether the trapezoidal of Simpson's rule is used.

[27]This is generally evident from the figures, but is also more specifically indicated by the values for the very large momentum components for $n_b = 5$ which correspond to the minimum occupation of one particle/bin.

[28]S. Nagamiya, I. Tanihata, S. Schnetzer, L. Anderson, W. Brückner, O. Chamberlain, G. Shapiro, and H. Steiner, J. Phys. Soc. Jpn. Suppl. 44, 378 (1978); S. Nagamiya, 4th High Energy Summer Study (Ref. 1), p. 71.

[29]Our results for group I, within the accuracy available with our statistics, are not inconsistent with the firestreak model, but of course do not test this.

[30]See, e.g., M. Gyulassi, presented at the Topical Conference on Large Amplitude Collective Nuclear Motion, Kesthely, Hungary, 1979 (LBL Report No. LBL-9244).

[31]J. Stachel and P. Havas, Phys. Rev. D 13, 1598 (1976), and references cited therein, for Hamiltonian and Lagrangian formulations which are Lorentz invariant to order c^{-2} and which involve only particles interacting directly through potentials.

[32]A reasonable fit is obtained with $\mu_A = 2.40$ fm^{-1} and with the other parameters following Eq. (1) remaining the same. It is interesting—although probably not too significant—that a better fit to $\sigma^{(2)}$ is obtained with V_{rel} than with V_{st}; in particular, V_{rel} gives a more nearly constant $\sigma^{(2)}$ at higher energies, in better agreement with the empirical values than does V_{st} (See Refs. 8 and 13). The retarded term V_{ret} generally gives a net repulsive contribution which increases with energy.

[33]In addition to conservation of energy E, momentum $\vec{P}$ and angular momentum $\vec{L}$, which follow from invariance of H with respect to time and space displacements and rotations, there is conservation to $O(v^2/c^2)$ of $\vec{K} = M\vec{R} - t\vec{P}$, corresponding to conservation of c.m. velocity, which follows from the invariance to $O(v^2/c^2)$ of H with respect to boosts. $\vec{R}$ is the c.m. position and M is the total mass which includes both the kinetic energy to $O(v^2/c^2)$ and the nonrelativistic potential energy. Thus $M\vec{R} = \sum_{i=1}^{A} m_i^* \vec{x}_i$ with $m_i^* = m_i(1 + p_i^2/2m^3c^2) + (1/2c^2)\sum_{i \neq j}^{A} V_{st}(r_{ij})$. The condition $\vec{K} = 0$ together with $\dot{M} \approx \dot{H} = 0$ (conservation of energy) and $\vec{P} = 0$ (conservation of momentum) then gives $\vec{R} = \vec{P}/M = \text{const}$, i.e. conservation of c.m. velocity. In our relativistic calculations, $\vec{K}$ was in fact found to be conserved with an accuracy which was consistent with the order v^2/c^2 of the calculations. It should be noted that $E = H$, $\vec{P}$, and $\vec{L}$ are exactly conserved for Hamilton's equations appropriate to H given by Eq. (10), since H satisfies all the corresponding invariances exactly.

[34]R. Babinet and L. Wilets, Univ. of Washington report (unpublished).